Inversion of Pulsed NMR Data Using Eigenanalysis

by

Wona Chung

Submitted to the Department of
Electrical Engineering and Computer Science
in partial fulfillment of the requirements for
the degrees of

Master of Science in Electrical Engineering and Computer Science

and

Bachelor of Science in Electrical Science and Engineering

at the

MASSACHUSETTS INSTITUTE OF TECHNOLOGY

May 1993

Author_____
Department of Electrical Engineering and Computer Science
May 1993

Certified by_____
Dr. Robert Freedman
Schlumberger Houston Products Center
Thesis Supervisor

Certified by_____
William M. Siebert
Ford Professor of Engineering
Thesis Advisor (Academic)

Accepted by_____
Campbell S. Searle
Chairman, Department Committee on Graduate Students

Inversion of Pulsed NMR Data Using Eigenanalysis

by

Wona Chung

Submitted to the Deparment of
Electrical Engineering and Computer Science
on 14 May 1993, in partial fulfillment of
the requirements for the degrees of
Master of Science in Electrical Engineering and Computer Science
and
Bachelor of Science in Electrical Science and Engineering

Abstract

Pulsed NMR technology is applied to fluid-saturated rocks to detect the presence of fluids in earth formations. The observed NMR signal is fit to a multi-exponential relaxational model, with a distribution of relaxation times corresponding to the distribution of pore sizes in a typical rock matrix. The inversion of this multi-exponential relaxation data is investigated.

Mathematically, the inversion problem is cast in the form of a Fredholm integral equation of the first kind. Decomposition of the measurement kernel reveals only a small subset of nonzero eigenvalues, a reflection of the high degree of redundancy in the data. The inversion is thus formulated as a linear combination of eigenfunctions corresponding to the non-zero eigenvalues of the kernel.

Typical of inversion problems, the solutions obtained are numerically unstable. Approximate solutions can be obtained using only the dominant eigenvalues, excluding the oscillatory eigensolutions belonging to very small eigenvalues. Although these solutions are stable, they cannot recover high frequency content.

Regularization theory allows the solutions to include all eigensolutions corresponding to nonzero eigenvalues. Although these solutions are also non-unique, they allow more detail in the distributions without forfeiting stability. A method for selecting an approximately optimal regularization parameter in a data-dependent manner is developed.

The inversion and optimal regularization algorithms were implemented and tested both on synthetic data and data collected by a prototype pulsed NMR tool.

Thesis Supervisor: Dr. Robert Freedman
Title: Schlumberger Houston Products Center

Thesis Supervisor: William M. Siebert
Title: Ford Professor of Engineering

Acknowledgments

Over the last three years, I have been privileged to supplement my academic studies with internships at Schlumberger. This thesis is comprised of research performed over the last year at the Houston Products Center and represents the culmination of my work in the electrical products group. By its nature, research cannot be performed successfully by a single individual, and I owe my gratitude to several generous persons.

I would like to thank my mentor at Schlumberger, Dr. R. Freedman, for supervising my thesis research. His work laid the foundation for this study, and my initiation into the project was aided singlehandedly by his generosity of time and knowledge. His approachability and understanding in the face of seemingly obvious and sometimes not so obvious questions are deeply appreciated. His expertise provided direction and insight throughout the project, and our discussions were invaluable to the progress of this work. He painstakingly read and corrected numerous revisions of this document with unbelievable patience. A hearty thank you for everything!

I thank Professor W.M. Siebert for advising this thesis on the academic end. His interest and comments at various stages in the project are gratefully acknowledged.

I am grateful to Dr. M. Ekstrom and J. Hunka for giving me the opportunity to join the PNMT group and securing generous funds to make my stay possible and comfortable.

My close friends deserve a special thanks for their valued friendship and support, reminding me to maintain a sense of humor at all times. They, as much as anyone, have made this thesis possible.

Finally, I owe my deepest thanks to my parents, who by example taught me the meaning of *hard work*. It is to them that I dedicate this thesis.

Contents

List of Figures

Chapter 1

Introduction

1.1 Background

In the well-logging industry, highly sophisticated tools are developed to extract petrophysical information about the earth formation. Oil companies and interpretation experts often use several different types of tools to investigate a borehole, each device designed to test for a property desirable in a producible well. The information obtained can then be pooled to judge the worthwhileness of drilling a well for commercial production.

Although there are numerous petrophysical properties which help determine the probability of finding oil, the focus of our treatment is porosity. Defined as the ratio of pore volume to total volume, porosity is a fundamental consideration when searching for possible sources of hydrocarbons. Pore space in a formation is filled with fluid, and hence a measure of porosity determines the availability of volume space for the existence of fluid in a formation. Once the presence of fluid is detected, methods exist to further investigate the rock to decipher the type of fluid present. Clearly, for petroleum exploitation purposes, a rock must be porous.

A borehole logging tool is currently being developed by Schlumberger Well Services for porosity estimation. The Pulsed Nuclear Magnetism Tool (PNMT) relies on the physics of NMR and works much like radar. Pulses of rf power are sent into the formation, and the returning pulses, or "spin-echoes", reflect the nuclear magnetic

relaxation rates of hydrogen atoms in the pore space of rocks. The tool takes advantage of the important fact that the tool is sensitive only to hydrogen atoms in fluids, not to hydrogen atoms in the solid matrix.

Only in exceptional cases, if at all, does the nature of practical measurements allow any tool to directly determine a desired quantity. For the PNMT, as in most cases, the measurement is indirect. Once data is collected, it is essential to accompany the measurement with some form of processing to infer useful information from the measured data. It is here where the scope of this thesis begins. We begin with pulsed NMR data, model the measurement process, and develop an algorithm to meet our ultimate goal of porosity estimation.

1.2 Motivation

While pulsed NMR is not a new technology, its application to wellbore exploration is a recent venture. In the past, NMR has been widely used in the medical field. Our study is particularly interesting because this well-established technology is applied to a completely different area. The mathematical puzzle which arises from describing the process analytically is very similar to another well-studied field, remote sensing. The prototype PNMT offers a unique opportunity to apply the mathematics of inversion to a difficult technical problem in a new setting.

The purpose of our study is, firstly, to develop a signal processing algorithm to estimate porosity in a formation from pulsed NMR data. Results will be benchmarked against existing solutions due to Freedman [7] and Sezginer [17] for accuracy and computational efficiency. Our academic, and equally important, goal is to study the underlying mathematics rigorously and derive a strategy for insuring that the solutions obtained are numerically stable.

1.3 Outline

Regardless of the type of measurement, success of information extraction relies largely on the experimenter's understanding of the measurement process. In this light, Chapter 2 begins our presentation with a review of the basic principles of NMR. The physics sets the basis for the measurement and explains the model chosen for the data.

Chapter 3 establishes the mathematical background used in the inversion algorithm. Inversion problems have been studied for decades, and the accepted equations to model them are introduced. The nature of instabilities, which complicates the inversion process, are studied. A highly acclaimed cure, the method of regularization, is discussed.

The derivation of the solution is outlined in Chapter 4. We obtain a likelihood function for a set of random variables derived directly from the collected data. The standard minimization of the likelihood function simplifies our problem into a linear set of equations. The formal solution is a linear combination of weighted eigenfunctions of the measurement kernel. In practice, this direct inversion is highly unstable.

Eigenanalysis, or a study of the eigenvalues and associated eigenvectors, of the measurement kernel suggests that the small (or nearly zero) eigenvalues need to be treated to cure the solution of wild oscillations. One method suggested in past literature is to simply exclude those terms which would contribute undesirable behavior. The limitation in this method is that the solution would be too smooth, and high frequency content would be excluded altogether. The regularization method allows high frequency resolution and at the same time augments tiny eigenvalues which caused difficulties in the formal solution. These solutions are not unique, and are in effect solutions to a constrained inversion problem.

Representative examples of our inversion algorithm are included. These examples were obtained using both synthetic and real data.

Finally, the results of this thesis are summarized in Chapter 5, and relative merits and limitations of the approach taken are considered. General conclusions are drawn which may be applicable to research in related applications.

Chapter 2

Data Acquisition

This introductory chapter, based on Abragam [1] and Farrar and Becker [6], reviews some basic NMR concepts in an attempt to facilitate understanding of the behavior of nuclear magnets in pulsed experiments. Quantitative analysis is included to supplement our qualitative discussion of NMR principles. Establishment of the underlying physics leads to a presentation of the data acquisition specifics and the relaxational model used in this study.

2.1 Basic Principles of NMR

NMR methods rest on the fact that the nuclei of many materials have a magnetic moment and an angular momentum, or "spin." The magnetic moments, equivalent to tiny magnetic dipoles, are magnetized with applied magnetic fields. They absorb electromagnetic energy from bursts of radio frequency (rf) power which perturb the equilibrium state. Observation of the transient spin system and intrinsic relaxation mechanism is used to extract information about the material being tested.

2.1.1 Relaxation and Nuclear Precession

A rock matrix typically contains pores of various sizes and shapes which can contain fluid. At the onset there is no net magnetization since the moments have random orientation (see figure 2-1).

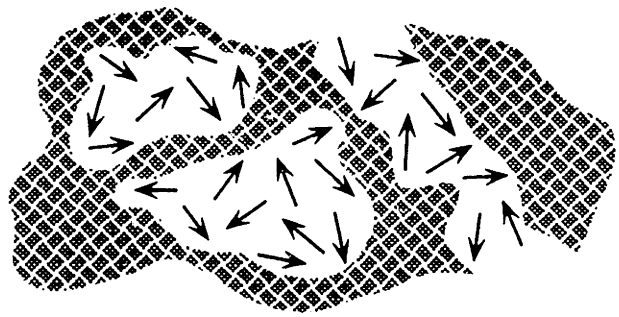

Figure 2-1. Sample of porous rock. Moments are randomly oriented in the fluid.

An applied static field in the z direction causes the moments to line up along the z-axis, and the material as a whole will be magnetized to some degree (see figure 2-2). The net magnetization is proportional to the applied field.

$$\mathbf{M} = \chi \mathbf{H_0} \tag{2.1}$$

where χ is the proton magnetic susceptibility.

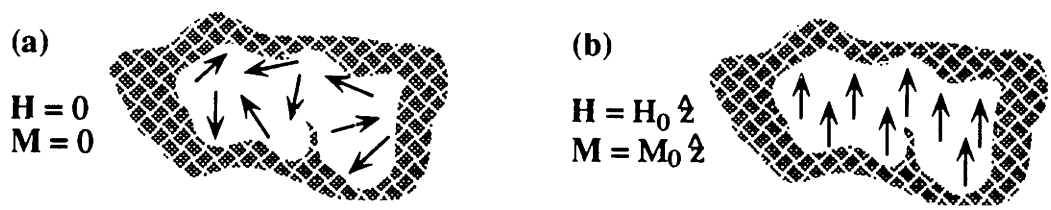

Figure 2-2. (a) Moments are randomly oriented in absence of applied field.
(b) Moments line up along direction of applied static field; object as a whole is magnetized to some degree.

The situation depicted in figure 2-2b is the equilibrium situation for NMR experiments. If this equilibrium is perturbed, i.e. the moments are tipped from their alignment with $\mathbf{H_0}$), the torque exerted by $\mathbf{H_0}$ on a moment inclined at an angle θ relative to $\mathbf{H_0}$ will cause the moment to precess about the z axis (see figure 2-3a) with a frequency given by the well-known Larmor equation:

$$\omega_L = -\gamma \mathbf{H_0} \qquad (rad\ sec^{-1}) \tag{2.2}$$

γ is the proton gyromagnetic ratio.

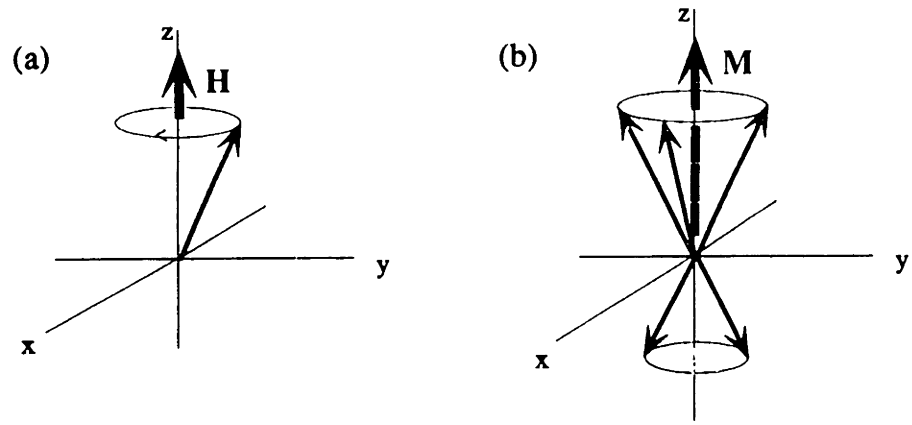

Figure 2-3. (a) Precession of a single moment μ about H when disturbed from equilibrium alignment.
(b) Ensemble of moments, each precessing about H at the Larmor frequency. A macroscopic magnetization M is defined as the vector sum of individual moments.

Study of a single moment (or spin), however, is not useful. Instead, an ensemble of a large number of nuclei, each precessing at the Larmor frequency about $\mathbf{H_0}$, is considered as an entity (see figure 2-3b). We define a net magnetization vector **M** as the sum of the individual moments. All following discussions will refer exclusively to the macroscopic magnetization **M**.

Following perturbation, the spin system we have just described will relax back to the equilibrium condition, where **M** is again aligned with the applied field. The relaxation mechanism is described by two first-order processes. The *spin-lattice* or *longitudinal relaxation time* T_1 accounts for the way the spin system returns to equilibrium with its surroundings and builds up magnetization in the z-direction. A second *spin-spin* or *transverse relaxation time* T_2 describes how the spins come to equilibrium with each other, effecting decay of magnetization in the x-y plane.

Before continuing with this qualitative presentation, we introduce the Bloch equations, which are useful to describe the behavior of **M** in pulse experiments.

2.1.2 The Bloch Equations

Bloch *et al* [1] derived a set of differential equations to explain the motion of the macroscopic magnetization **M** in the presence of an applied field. The classical equation of motion of **M** in a field **H** is as follows:

$$\frac{d\mathbf{M}}{dt} = \gamma \mathbf{M} \times \mathbf{H} \tag{2.3}$$

In general, **H** consists of both a static applied field $\mathbf{H_0}$ and an rf field linearly polarized along the x-axis. The latter can be thought of as two circularly polarized fields, rotating in opposite directions with respect to each other:

$$\mathbf{H_1} = \underbrace{H_1 \cos\omega t\,\hat{x} - H_1 \sin\omega t\,\hat{y}}_{H_-} + \underbrace{H_1 \cos\omega t\,\hat{x} + H_1 \sin\omega t\,\hat{y}}_{H_+} \tag{2.4}$$

H_+ rotates counter to the precessing moments and can be ignored since it does not meet the resonance condition (refer to Abragam [1]). Only H_- contributes, and the components of **H** are:

$$H_z = H_0 \tag{2.5a}$$

$$H_x = H_1 \cos\omega t \tag{2.5b}$$

$$H_y = -H_1 \sin\omega t \tag{2.5c}$$

Equations (2.3) and (2.5) can be combined into differential equations for each component of **M**. The complete Bloch equations, including relaxation terms, are as follows:

$$\frac{dM_x}{dt} = \gamma(M_y H_0 + M_z H_1 \sin\omega t) - \frac{M_x}{T_2} \tag{2.6a}$$

$$\frac{dM_y}{dt} = \gamma(M_z H_1 \cos\omega t - M_x H_0) - \frac{M_y}{T_2} \tag{2.6b}$$

$$\frac{dM_z}{dt} = -\gamma(M_x H_1 \sin\omega t + M_y H_1 \cos\omega t) - \frac{(M_z - M_0)}{T_1} \tag{2.6c}$$

The Bloch equations above can be solved analytically in the laboratory frame of

reference, but details are, in general, laborious. They are more easily solved in a rotating frame of reference.

2.1.3 The Rotating Frame of Reference

Pulse phenomena are best observed in a coordinate system which rotates about $\mathbf{H_0}$ at the Larmor frequency. In this new coordinate system, called the rotating frame, the x′ and y′ axes rotate about the z′ axis (see figure 2-4). The spin motion of M, when perturbed by other applied fields, delineates very complex paths in the fixed laboratory frame. In the fixed frame, steady precession about H_0 must be superimposed on another (slower) precession induced by a second field which will be introduced shortly. The spin motions can be derived in much simpler forms in the rotating frame, which in effect eliminates the Larmor precession about $\mathbf{H_0}$. This simplification can be readily appreciated when mathematics are introduced.

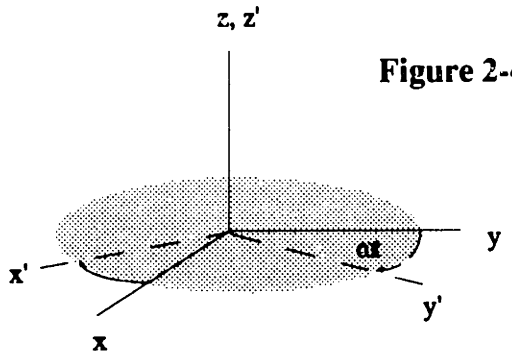

Figure 2-4. The axes of the rotating frame (x', y', z') rotate about the fixed frame (x, y, z) with angular frequency ω.

The overall motion of M in the lab frame can be related to its motion in the rotating frame, where rotation of the axes is mathematically described in terms of a vector cross product:

$$\left(\frac{d\mathbf{M}}{dt}\right)_{\substack{fixed\\frame}} = \left(\frac{\partial \mathbf{M}}{\partial t}\right)_{\substack{rotating\\frame}} + \vec{\omega} \times \mathbf{M} \qquad (2.7)$$

Making use of (2.3) and simplifying yields:

$$\left(\frac{\partial \mathbf{M}}{\partial t}\right)_{rot} = \gamma \mathbf{M} \times \left(\mathbf{H} + \frac{\vec{\omega}}{\gamma}\right) \tag{2.8}$$

Furthermore, an *effective* field can be defined:

$$\left(\frac{\partial \mathbf{M}}{\partial t}\right)_{rot} = \gamma \mathbf{M} \times \mathbf{H_{eff}} \tag{2.9}$$

$$\mathbf{H_{eff}} = \mathbf{H} + \frac{\vec{\omega}}{\gamma} = (\mathbf{H_0} + \frac{\vec{\omega}}{\gamma}) + H_1 x' \tag{2.10}$$

where the term $\frac{\omega}{\gamma}$ can be considered a fictitious field arising from effects of the rotation. The significance of (2.10) is that it points out the validity of the ordinary Bloch equations even in the rotating frame, provided $\mathbf{H_{eff}}$ is used in place of $\mathbf{H}$. Notice we are now left with two static fields.

2.1.4 Spin Tipping in the Rotating Frame

Consider the equilibrium situation with an applied static magnetic field $\mathbf{H_0} = \mathbf{H_0}\,\hat{\mathbf{z}}$. Pulses of radio frequency (rf) fields $\mathbf{H_1}$, applied at right angles to $\mathbf{H_0}$, perturb the equilibrium. Energy is absorbed from $\mathbf{H_1}$ only when its frequency satisfies the resonance condition:

$$\omega = \omega_L \tag{2.11}$$

By choosing our rotating coordinate system with

$$\vec{\omega} = -\gamma \mathbf{H_0} \tag{2.12}$$

(2.10) simplifies to give us only an rf field, which appears static in the rotating frame, to interact with $\mathbf{M}$.

$$\mathbf{H_{eff}} = \mathbf{H_1} \tag{2.13}$$

Initial conditions, then, are:

$$M'_x(0) = M'_y(0) = 0 \tag{2.14a}$$

$$M'_z(0) = M_0 \tag{2.14b}$$

The equations of motion reduce to:

$$\frac{dM'_x}{dt} = -\frac{M'_x}{T_2} \tag{2.15a}$$

$$\frac{dM'_y}{dt} = \gamma M'_z H_1 - \frac{M'_y}{T_2} \tag{2.15b}$$

$$\frac{dM'_z}{dt} = -\gamma M'_y H_1 - \frac{(M'_z - M_0)}{T_1} \tag{2.15c}$$

For rf pulses of short duration compared to the relaxation times, relaxation effects can be neglected. Solutions for short rf pulses of duration τ (i.e., $\tau(\tau \ll T_2 \leq T_1)$ the solution to the above set of equations is:

$$M'_x(\tau) = 0 \tag{2.16a}$$

$$M'_y(\tau) = M_0 \sin \omega_1 \tau \tag{2.16b}$$

$$M'_z(\tau) = M_0 \cos \omega_1 \tau \tag{2.16c}$$

Equations 2.16 show that, in the rotating frame, an applied rf field $\mathbf{H_1}$ results in precession of $\mathbf{M}$ about $H_1 \hat{x}'$. $\mathbf{M}$ remains in the $y' - z'$ plane, and the angle of rotation is

$$\theta = \omega_1 \tau = \gamma H_1 \tau \tag{2.17}$$

Rate of precession remains constant at the Larmor frequency, but the angle of rotation can be chosen by the experimenter using the above relation. Figure 2-5 shows the magnetization vector being tipped by an rf field. The most common tipping pulses are for 90° and 180° angles of rotation.

Figure 2-5. **M** being tipped by 90° and 180° pulses, respectively.

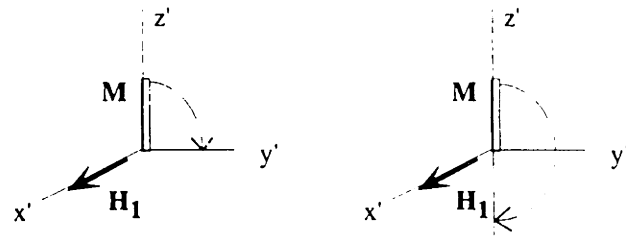

In the fixed frame, the motion of **M** is far more complex. While the moments are being tipped toward the x-y plane, they would also be precessing about the z axis. The rotating frame travels with the precession, and only the tipping needs to be considered.

2.1.5 Relaxation in the Rotating Frame

After **M** has been tipped to the desired angle, $\mathbf{H_1}$ is turned off to observe the nuclear spin system. Recall that $\mathbf{H_0}$ is a permanent static field and is still on. **M** has been tipped to the y′ axis with a $\frac{\pi}{2}$ pulse, and the initial conditions can be stated as:

$$M'_y(0) = M_0 \tag{2.18a}$$

$$M'_x(0) = M'_z(0) = 0 \tag{2.18b}$$

The equations of motion now simplify to:

$$\frac{dM'_x}{dt} = -\frac{M'_x}{T_2}, \tag{2.19a}$$

$$\frac{dM'_y}{dt} = -\frac{M'_y}{T_2}, \tag{2.19b}$$

$$\frac{dM'_z}{dt} = -\frac{(M'_z - M_0)}{T_1}, \tag{2.19c}$$

and the solutions of the Bloch equations in the rotating frame are:

$$M'_x(t) = 0, \tag{2.20a}$$

$$M'_y(t) = M_0 \exp(-t/T_2), \tag{2.20b}$$

$$M'_z(t) = M_0\,[1 - \exp(-t/T_1)]. \tag{2.20c}$$

2.1.6 Solutions in the Fixed Frame

The solutions of the Bloch equations in the fixed frame are obtained simply by applying a transformation matrix to carry the results between frames of reference. The components in the fixed frame can be simply related to their counterparts in the rotating frame (denoted by primes) by the following:

$$\begin{pmatrix} M_x \\ M_y \\ M_z \end{pmatrix} = R^{-1} \cdot \begin{pmatrix} M'_x \\ M'_y \\ M'_z \end{pmatrix} \tag{2.21a}$$

(2.21b)

$$R^{-1} = \begin{pmatrix} \cos\omega t & \sin\omega t & 0 \\ -\sin\omega t & \cos\omega t & 0 \\ 0 & 0 & 1 \end{pmatrix} \tag{2.21c}$$

The relaxation process, after a $\frac{\pi}{2}$ rf pulse has been applied and subsequently turned off, follows directly from (2.20) and (2.21):

$$M_x(t) = M_0 \sin\omega_0 t \exp(-t/T_2) \tag{2.22a}$$

$$M_y(t) = M_0 \cos\omega_0 t \exp(-t/T_2) \tag{2.22b}$$

$$M_z(t) = M_0\,[1 - \exp(-t/T_1)] \tag{2.22c}$$

Equations 2.22 describe how **M** precesses about the static field $\mathbf{H_0}$ and simultaneously returns to its equilibrium position in the z direction. The transverse components of **M**, M_x and M_y, decay exponentially to their equilibrium value of zero with a time constant T_2, or "spin-spin relaxation time". If local field inhomogeneities of the static field $\mathbf{H_0}$ are significant, the transverse magnetization decays with a faster time constant T_2^*. Inhomogeneities cause each moment to precess at a slightly different

frequency, causing dephasing of M_x and M_y (see figure 2-6). This in turn speeds up the decay of transverse magnetization.

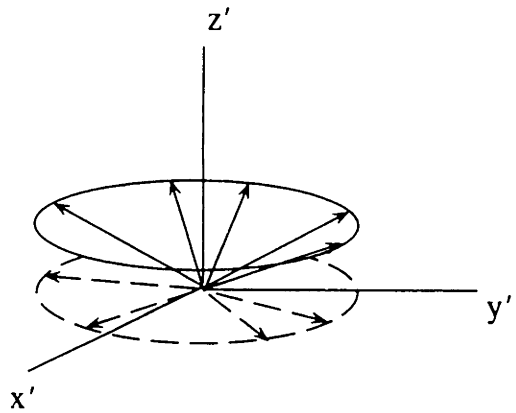

Figure 2-6. Moments dephase in the x'-y' plane, and magnetization in the z' direction diminishes.

The longitudinal component of **M**, M_z, will return to its equilibrium value M_0 with a time constant T_1, or "spin-lattice relaxation time". The rate with which M_z builds up is governed by molecular properties of the fluid and its environment within the rock pore space.

Clearly, if **M** has returned to its equilibrium value $M_o\hat{z}$ there can be no component of **M** in the $x-y$ plane. Hence T_2, the time describing loss of M_x and M_y, can never be longer than T_1, the time characterizing restoration of M_z. In general, then,

$$T_2^* \leq T_2 \leq T_1. \tag{2.23}$$

2.2 Apparatus and Measurement Technique

2.2.1 PNMT

Conventional NMR methods have been studied since the 1940's, and prior applications have not necessitated revision of conventional laboratory NMR devices. Our application, however, cannot make use of the conventional devices that place the material being tested inside a magnet and rf coil. The prototype PNMT, based on a novel "inside-out" design created by Kleinberg *et al* [12], meets the need for mea-

surements on large samples such as the earth formation (see figure 2-7). The field is predominantly radial and is relatively homogeneous only inside the small dashed square. The instrument also has its own radio frequency antenna which generates oscillating rf fields perpendicular to the static field. Refer to Kleinberg for details concerning the NMR apparatus used for the data in this study.

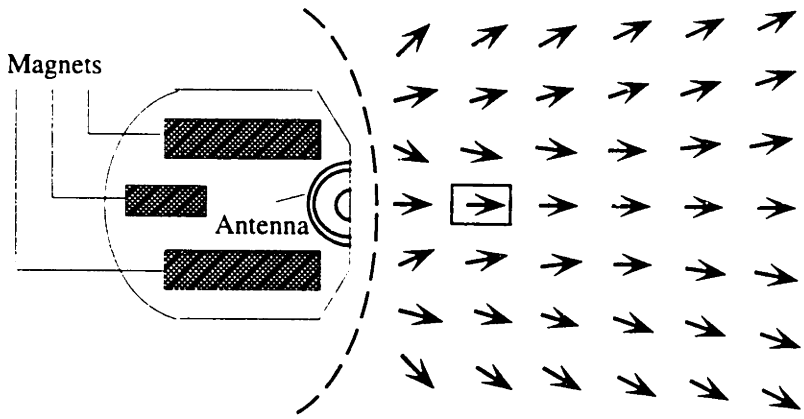

Figure 2-7. Adapted from Kleinberg *et al* [1991]. Cross-section of the "inside-out" NMR apparatus. Arrows indicate direction of the static magnetic field into the borehole. The field is relatively homogeneous inside the small square in the earth formation.

2.2.2 CPMG Technique

The spin-echo measurement sequence used by the PNMT is the Carr-Purcell sequence with the Meiboom-Gill modification (CPMG). The rationale of the CPMG method is shown in figure 2-8. In (a) **M** is shown being tipped through 90° by an applied rf field $\mathbf{H_1}$. Following removal of the rf field, the individual nuclei experience slightly different values of the static field, and hence their frequency of precession will differ slightly. Some nuclei travel faster, and some slower, than the rotating frame, and hence as a collection the nuclei will fan out. For simplicity, the rate of frame rotation is taken to be slower than the rotation frequency of the moments m_i, and hence the moments are depicted rotating in a single direction. In (c), at a time t_{cp} after the 90° pulse, a 180° pulse is applied along the y′ axis, which flips each moment by 180°

about the y′ axis. The moments continue to travel as shown in (d), and rephase to produce an "echo", as shown in (e). In (f), the moments are shown dephasing again, and the cycle (c)-(f) continues as 180° pulses of rf power are applied at odd multiples of t_{cp}, and echoes collected at even multiples of t_{cp}.

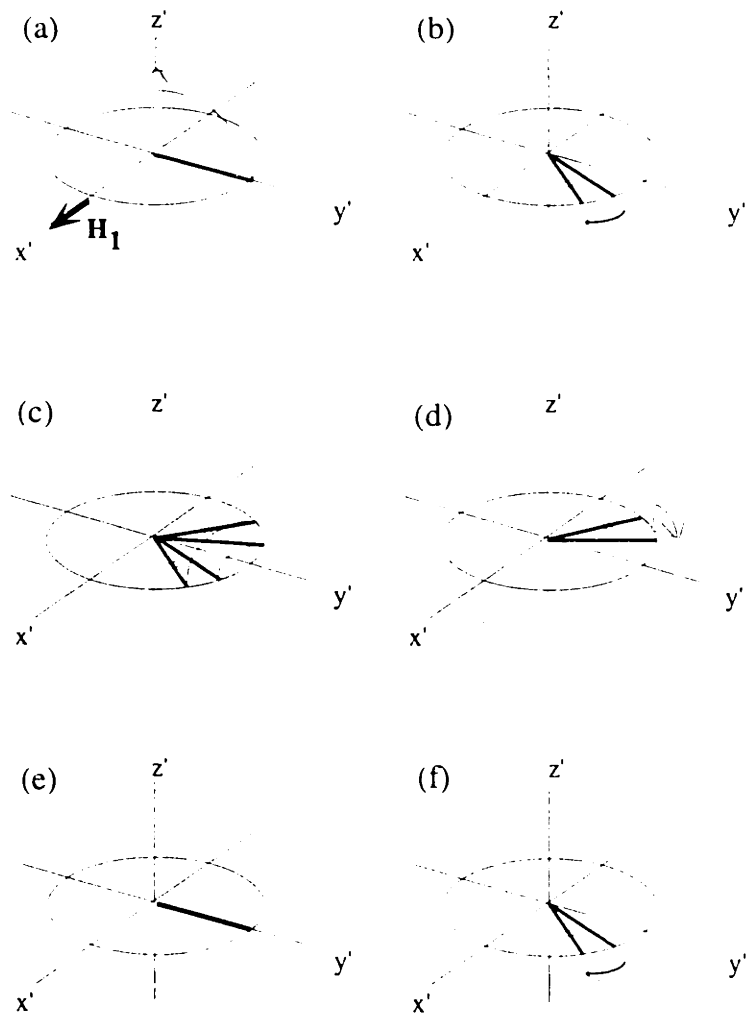

Figure 2-8. The CPMG technique, taken from Farrar and Becker [1971]. For clarity, the frame's rate of rotation is taken to be slower than the precession frequencies of any of the moments. Thus all moments appear to move in the clockwise direction as viewed down the z' axis, but some move faster than others due to local field inhomogeneities.

An illustrative cartoon of the CPMG technique is given in figure 2-9. The signal is measured as voltage induced in an antenna, and the picture shows in a succinct fashion the relationships between the periodic pulses and received echoes.

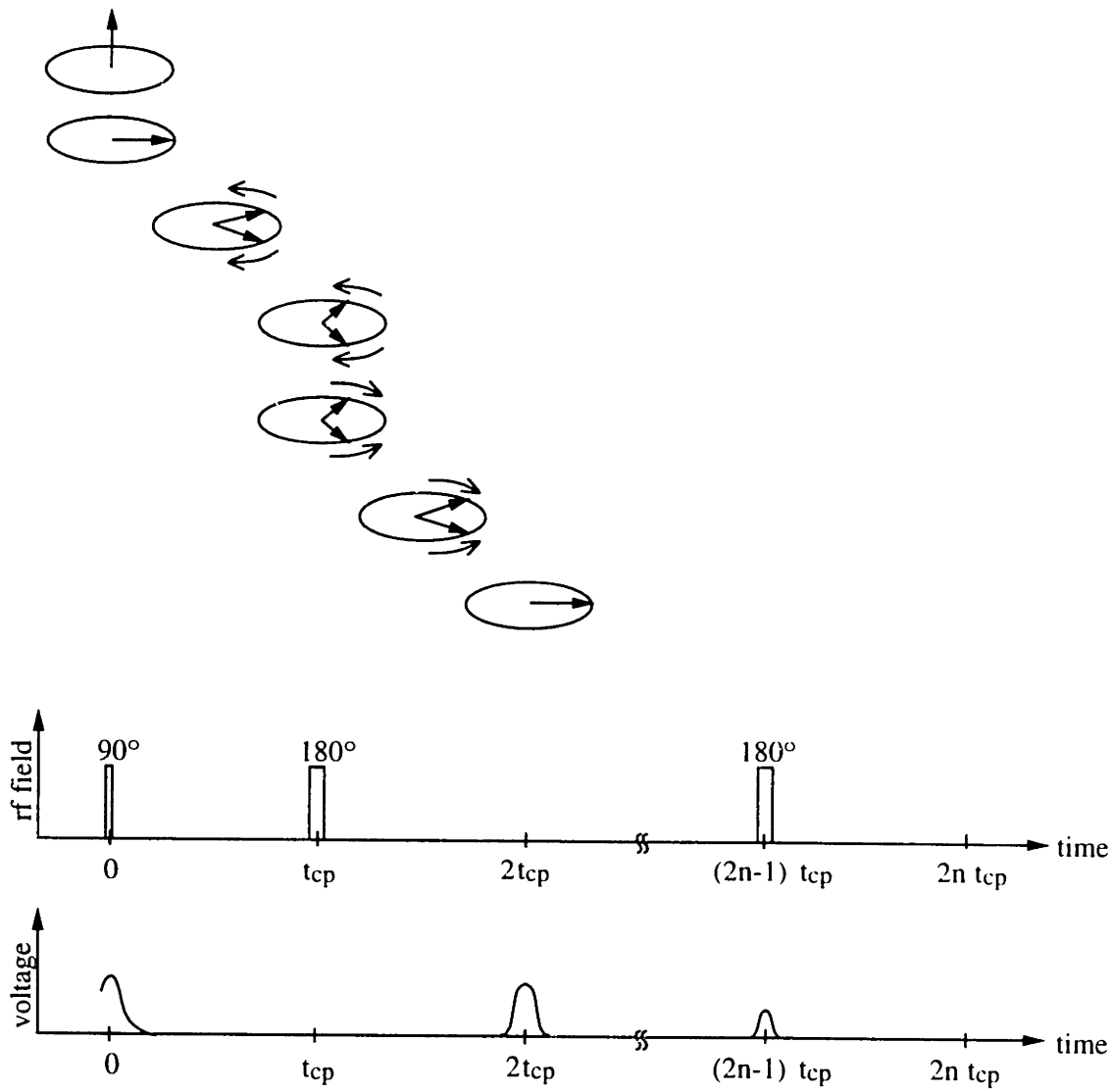

Figure 2-9. Cartoon illustrating CPMG technique

2.3 Multi-Exponential Decay Model

2.3.1 Definitions

Studies show that fluids which have a short relaxation time are trapped in small pores and/or are highly viscous. Hence bound fluids will not flow easily and are not easily extractable. Conversely, fluids which will flow easily under feasible pressure gradients, free fluids, relax with relatively long relaxation times.

An empirically determined cutoff relaxation time T_c separates the total porosity reading into "bound-fluid" and "free-fluid" porosities. Fluids with relaxation times less than T_c contribute to bound-fluid porosity ϕ_{bf}, and similarly fluids with relaxation times greater than T_c contribute to free-fluid porosity ϕ_{ff}. Only free-fluid porosity is of commercial interest.

2.3.2 Assumptions

NMR relaxation times are very sensitive to the molecular environment. Pore size is significant since surfaces hinder molecular motion. A distribution of pore sizes, typical in rock formations, is responsible for the distribution of relaxation times observed.

The signal to noise ratio of borehole PNMT measurements is poor. Thermal noise generated by the tool electronics corrupts the data. Experiments show that the noise can be modeled as additive, zero-mean, uncorrelated Gaussian noise.

2.3.3 Relaxational Model

The signal collected by the PNMT is a series of echoes reflecting the decay of proton nuclear magnetization of the fluids in rock pores. The decay of each echo is characterized by T_2^* due to field inhomogeneities in the rock. The larger envelope, shown by the dotted line in figure 2-10, describes the decay rate of the NMR signal characterized by T_2. Between successive 180° pulses, M_z has not had sufficient time to return to equilibrium. It is assumed that the net magnetization developed along the z-axis between pulses is negligible.

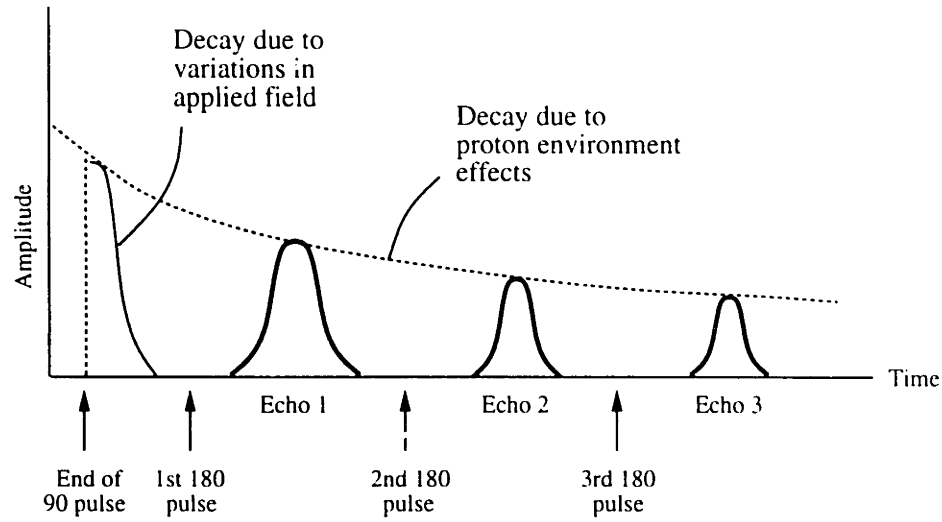

Figure 2-10. NMR spin-echo measurement

If a formation had only one pore, or pores of a single size, the decay of magnetization would be observed as a single exponential decay, the time constant being simply the relaxation time. Given the countless possible pore sizes in a formation, then, the relaxation will be characterized by a distribution of respective decay times. Depending on the complexity of the model, a selected number of weighted exponentials can be chosen to characterize the observed decaying signal, as illustrated in figure 2-11.

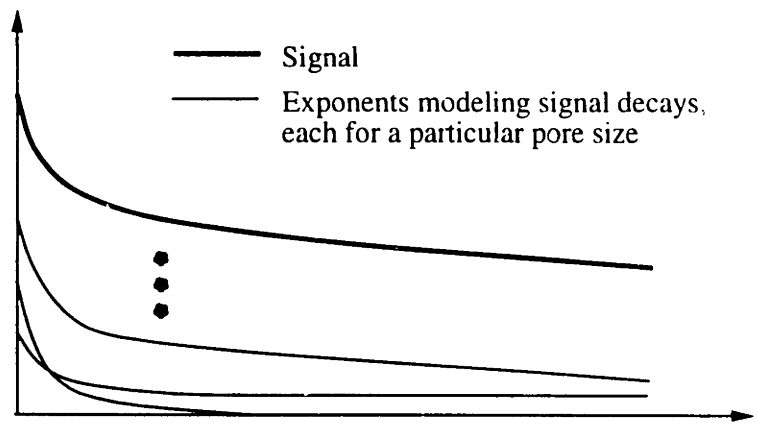

Figure 2-11. Multi-exponential relaxational model

The problem then becomes fitting the distribution of relaxation times to the observed decay curve. Figure 2-12 shows a typical CPMG echo sequence. The wide scattering in echoes shows the poor SNR inherent in the measurement. Our goal is to fit the exponentials to the NMR signal, shown by the solid line.

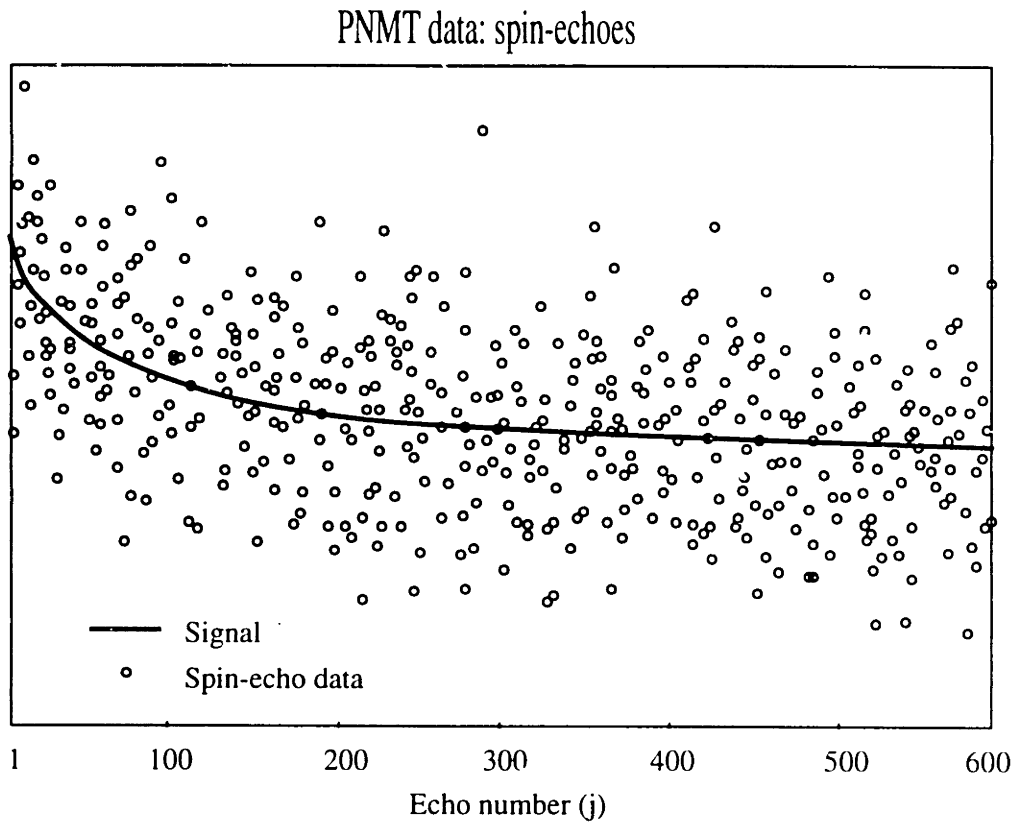

Figure 2-12. Signal super-imposed on collected spin-echo data

Chapter 3

Mathematical Background

This chapter introduces the fundamental integral equation of indirect measurement, the Fredholm integral equation of the first kind. In general, Fredholm equations are ill-conditioned and cannot be solved analytically. The theory of Tikhonov's regularization method is applied to approximately solve the ill-posed problem.

3.1 Inversion Problems

Interpretation of data obtained through indirect measurement is a classical inversion problem. Many practical examples, such as remote sensing, place severe demands on the ability of users to extract key information from measurement data. Clever schemes are necessary to truly "read" the data in any meaningful way.

In a generalized sense, we can define observables as parameters that can be measured physically. In contrast, we may define a set of natural parameters that are to be determined. The most important problem, then, is to find the *correct* relation between the observables and the natural parameters. The relation allows translation of the observables into the desired parameters, and the problem is solved. In practical situations, however, the relation can be very complicated, and exact solutions are not attainable.

The difficulties arise because the types of equations that describe many inversion problems are such that analytical solutions are out of the question. Routine numerical

techniques fail because, in general, the equations are ill-conditioned, a property which will be defined shortly. By using suitable approximations, we can obtain solutions that are useful and sufficiently accurate for certain applications.

3.2 Fredholm Integral Equations of the First Kind

Many inverse problems can be stated in the form of the well-known Fredholm integral equation of the first kind:

$$\int_a^b K(y,x)\, f(y)\, dy \;=\; g(x) + \varepsilon(x) \tag{3.1}$$

The elements of the model are as follows:

$K(y,x)$	:	measurement kernel (or known response function)
$f(y)$	:	unknown function which is sought
$g(x)$	:	data
$\varepsilon(x)$	:	error

The problem is to estimate the unknown function $f(y)$ based on the observed data, and a peculiar problem can be associated with the solution to (3.1). In Fredholm equations of the first kind, the mapping g $\rightarrow$ f is not continuous; that is to say, the solutions generally depend discontinuously on the data. Therefore small errors in the measured g may lead to enormous variations in the solution f, and the issue of uniqueness needs to be considered.

For implementation purposes, (3.1) is re-stated as a quadrature inversion by replacing the integrals by sums and is written in operator form:

$$\mathbf{K}\,\mathbf{f} = \mathbf{g} + \varepsilon \tag{3.2}$$

In general, the error in the quadrature operation is not large, especially when the functions involved are reasonably smooth. In fact, while quadrature does produce an error, the quadrature error is not the dominant factor in the overall uncertainty.

3.3 Solutions of the Fredholm equations of the first kind

Mathematicians have studied the Fredholm equations for several decades, and it is well accepted they are quite difficult to solve. Since the solution does not depend continuously on the data function, an exact inversion is doomed to fail. There are infinitely many solutions which satisfy a slight variant of the intrinsic integral equation, and it is common to seek "smooth" solutions rather than exact ones.

3.3.1 Direct inversion

An attempt to solve the system:

$$\mathbf{K}\,\mathbf{f} = \mathbf{g} \tag{3.3}$$

for $\mathbf{f}$ might lead one to try the obvious direct inversion:

$$\mathbf{f} = \mathbf{K}^{-1}\,\mathbf{g} \tag{3.4}$$

Mathematically speaking, the inverse matrix only exists when $\mathbf{K}$ is square and non-singular. In general, $\mathbf{K}$ does not satisfy these properties, and our direct approach fails miserably in practice. The resulting solution, if attainable, suffers from *instability*: small changes in $\mathbf{g}$ produce enormous changes in $\mathbf{f}$. The result is a wildly oscillating solution that is highly sensitive to noise.

The problem lies in the fact that $\mathbf{K}$ has small eigenvalues, a manifestation of the high degree of interdependence among adjacent rows and columns in the measurement kernel matrix. The small eigenvalues of $\mathbf{K}$ results in large elements in $\mathbf{K}^{-1}$, if the inverse exists, and the presence of these large elements inevitably produces instability.

There is also a problem of uniqueness. The matrix $\mathbf{K}$ is non-square, meaning the the system is under-determined. No unique solution exists.

3.3.2 Least squares problem

Another inversion approach is least squares optimization, where the best possible solution is chosen from a family of solutions. The best least squares solution, i.e. one which minimizes the norm of the residual $(\mathbf{K}\,\mathbf{f} - \mathbf{g})$, is given by

$$\mathbf{f} = (\mathbf{K}^{\mathrm{T}}\,\mathbf{K})^{-1}\,\mathbf{K}^{\mathrm{T}}\,\mathbf{g} \tag{3.5}$$

The symmetric matrix $\mathbf{K}^{\mathrm{T}}\,\mathbf{K}$ has an inverse; numerically, however, this inversion is still highly unstable. In fact, the solution given by the least squares method is no better that than obtained through direct inversion in regard to the problem of instability. In general, $\mathbf{K}^{\mathrm{T}}\,\mathbf{K}$ has even smaller eigenvalues than $\mathbf{K}$. Clearly, the eigenvalues need to be boosted in some way. Equivalently, a smoothing term is needed to stabilize the solution, and the method of choice has been regularization.

3.4 Regularization theory

Tikhonov's groundbreaking paper on the method of regularization for numerical solutions of Fredholm integral equations of the first kind received much attention in the 1960's. Intensive development of the theory of the method followed, and the method was quickly applied to a range of difficult technical problems. Regularization replaces the ill-posed problem by a stable minimization problem[14].

We now introduce Tikhonov's concept of *well-posedness* for such equations [11]. The inversion in (3.1) is said to be well-posed if

(a) for each $g \in x$, there is a solution $f \in y$
(b) the solution is unique in y
(c) f depends continuously on g

An equation which does not meet the above conditions is termed *ill-posed.*

The solution to the ill-posed least squares problem can be obtained by minimizing a likelihood function, with an added smoothing term. Thus the *constrained* linear

inversion problem becomes:

$$\mathbf{f} = argmin\,[\,(\mathbf{K}\,\mathbf{f} - \mathbf{g})^2 + \gamma\,(\mathbf{L}\,\mathbf{f})^2\,] \tag{3.6}$$

and the constrained least squares solution is

$$\mathbf{f} = (\mathbf{K}^T\,\mathbf{K} + \gamma\mathbf{L}^T\mathbf{L})^{-1}\,\mathbf{K}^T\,\mathbf{g} \tag{3.7}$$

where $\mathbf{L}$ denotes some linear operator. The operator reflects the application's definition of "smoothness." Phillips [16] defined smoothness via minimization of a second-difference expression and obtained favorable results. In general, a combination of several k-th differences, with appropriate weights applied to each constraint, can effect a particular form of smoothing.

The positive parameter γ, called a regularization parameter, penalizes large deviations of the solution $\mathbf{f}$ or its derivatives, depending on the choice of operator $\mathbf{L}$. The duty of this parameter is to effect a trade-off between smoothness (large γ) and fidelity in the approximate solution (small γ) [20]. The "goodness" of the solution, and the resulting choice of $\mathbf{L}$ is established by a selected criterion of desired smoothness.

The functions derived from the above likelihood function with the regularization term will be called a "regularized family of approximate solutions" [20]. Indeed, infinitely many solutions, for different choices of the regularization parameter γ, fit the set of linear equations. Selection of an appropriate γ involves a tradeoff between stability and accurate data-fitting. The best fit to the data is achieved by setting γ to zero; however, as previously discussed, the solution will be numerically unstable. A large value of γ yields very stable solutions at the expense of a bias which prevents solutions from fitting the data.

3.5 Method of Dominant Eigensolutions

The solution can be interpreted as projections of the measurement kernel onto a set of eigenvectors. Since highly oscillatory eigenvectors are associated with small eigenvalues, the method of restricting the solution to a set of dominant eigensolutions is a filtering process which excludes high-frequency contributions. This method of simply ignoring the smallest eigensolutions was studied by Baker, Fox, Mayers, and Wright [2]. Respectable results are obtained, especially when the distributions we are seeking are smooth in nature. Formally choosing where to determine the distinction for eigenvalues which are "dominant" will be addressed in the next chapter, and this choice is application-dependent.

We notice that this is a simple method which does not require regularization. The price we pay for the simplicity in the algorithm, though, is detail in the formal solution. The filtering employed by restricting the distribution to dominant eigensolutions is a crude one, and utilization of a regularization term can provide more detail in the distributions while providing numerical stability. In the next chapter, we will derive a solution based on the mathematical theory detailed above, and regularization, rather than the method of dominant eigenfunctions, will be used to stabilize the solutions.

Chapter 4

Derivation of Solution

The problem is cast in the form of a Fredholm integral equation of the first kind. Brute force methods to solve the integral equation are not computationally feasible due to the abundance of data collected in pulsed NMR measurements. Another critical problem concerns the numerical stability of the solutions. We begin our derivation with a data compression algorithm developed by Freedman [7]. A likelihood function is derived for the reduced data set (random variables) representing the collected spin-echoes, and standard minimization of the likelihood function leads to a system of linear algebraic equations. Formal solution to the linear system of equations is attacked using an eigenvalue analysis approach.

4.1 Pre-processing

4.1.1 Data Compression

Processing of CPMG data is difficult for two reasons: the need for extensive computational power, due to abundance of raw data, and poor signal to noise ratio. Freedman developed a pre-processing method to attack these difficulties. A set of signal-plus-noise echoes $A_j^{(+)}$ are derived from the original data set. Refer to [7] for details, including phase estimation and rms noise estimation.

The data compression scheme consists of defining non-overlapping windows across

the range of echoes, and simply summing the values of the echoes within each window:

$$\tilde{I}_m = \sum_{j=N_m}^{N_{m+1}} A_j^{(+)} \tag{4.1}$$

N_m and N_{m+1} are the endpoints of the m^{th} window. For simplicity, details to accommodate the classical fencepost problem faced in implementation has been omitted. See figure 4-1 for a pictorial representation of the data compression method.

The super-echoes, or sums of echoes within each window, are the new reduced data set. They can be interpreted as a weighted sum of amplitudes in the desired spectrum:

$$\tilde{I}_m = \sum_{l=1}^{N_s} a_l \, f_l \, F_m + \tilde{N}_m \tag{4.2}$$

where the weights are:

$$f_l = 1 - \exp(-W/(\zeta T_{2,l}))$$

$$F_m \sum_{j=N_m}^{N_{m+1}} \exp(-j\Delta/T_{2,l})$$

$$\tilde{N}_m = \sum_{j=N_m}^{N_{m+1}} N_j^{(+)}$$

f_l models incomplete recovery of the longitudinal magnetization during time W. F_m reflects the sensitivity of the m^{th} window to the components in the spectrum. Here we have used the approximation $\mathrm{T_1} = \zeta \mathrm{T_2}$, which holds for rocks. $N_j^{(+)}$ is obtained by summing the noise over time windows, using the data compression process described earlier. The noise is zero-mean, uncorrelated Gaussian noise with variance ψ. The time axis in the region of interest $[T_{2,min} \ldots T_{2,max}]$ is divided into equally spaced components on a logarithmic scale, and the unknown distribution are the weights a_l corresponding to each relaxation time $\mathrm{T_{2,l}}$. Refer to Freedman [7] for explicit derivations and details of this model.

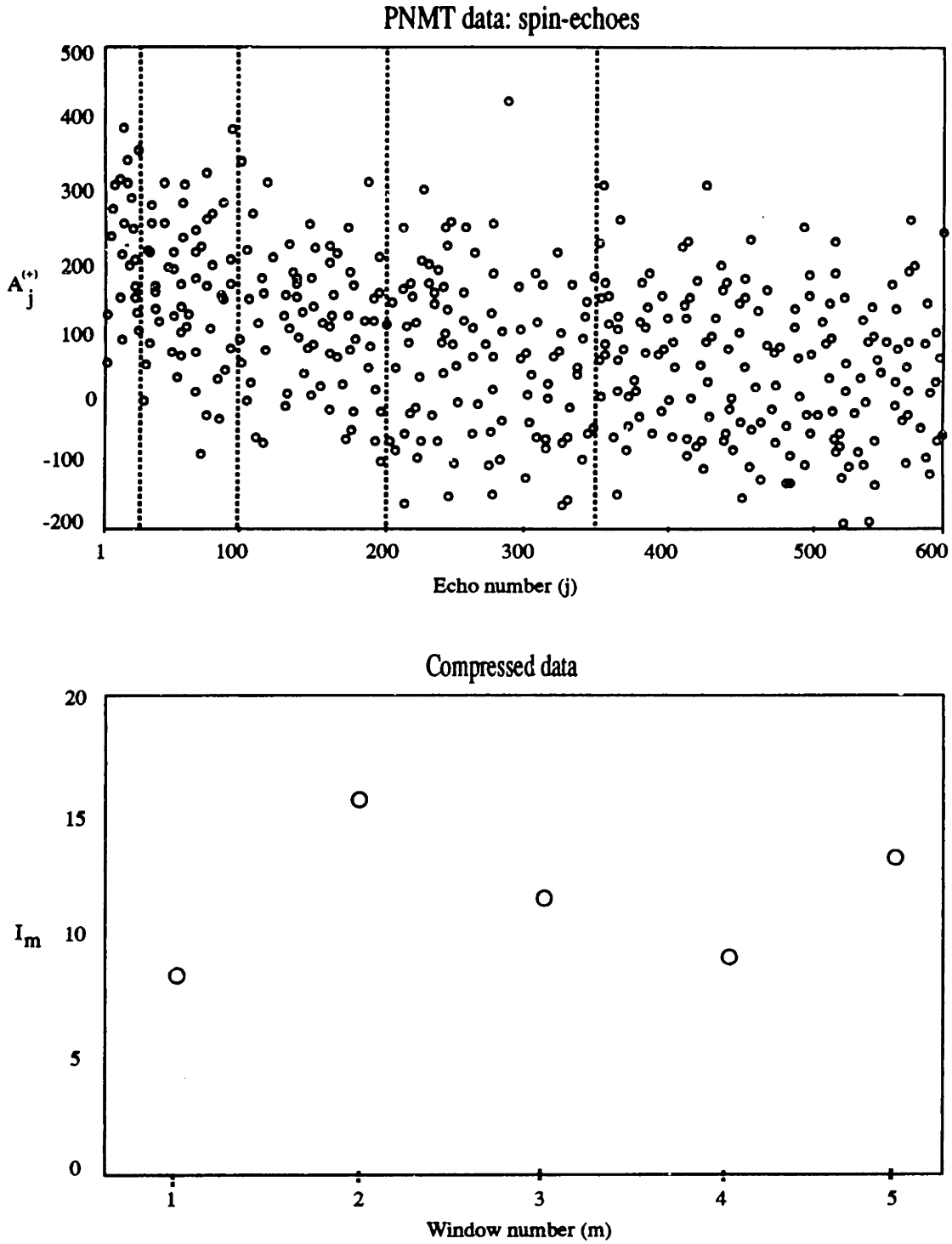

Figure 4-1. Data compression method: summation over time windows

The super-echoes $\tilde{I}_m$ are random variables with a known mean and variance. The variance in each window is the sum of variances in each echo (uncorrelated random variables), and hence reduces to the length of the window (ie, number of echoes in the window) multiplied by the variance in a single echo, ψ.

$$< \tilde{I}_m > = \sum_{l=1}^{N_s} a_l f_l F_m \equiv I_m\{a_l\} \tag{4.3}$$

$$\sigma^2(\tilde{I}_m) = d\psi(N_{m+1} - N_m) \equiv \psi\hat{\sigma}_m^2 \tag{4.4}$$

4.1.2 Likelihood Function

A likelihood function is written for the Gaussian random variables $\tilde{I}_m$ as follows:

$$-\ln \mathbf{L} = \sum_{m=1}^{N_w} \frac{(\tilde{I}_m - I_m\{a_l\})^2}{2\psi\hat{\sigma}_m^2} \tag{4.5}$$

Stability can be ensured, as discussed in Chapter 3, by adding a regularization constant:

$$-\ln \mathbf{L} = \sum_{m=1}^{N_w} \frac{(\tilde{I}_m - I_m\{a_l\})^2}{2\psi\hat{\sigma}_m^2} + \frac{\gamma}{2\psi}\sum_{l=1}^{N_s} a_l^2 \tag{4.6}$$

The regularization term imposes a penalty for large amplitude deviations, behaving as a smoothing filter on the solution. In this case we have chosen the operator to be the L_2 norm.

Solving the problem in the form of a maximum likelihood function is in fact equivalent to mean square error estimation. The mean square error criterion results in optimum or near optimum performance in comparison with other measures. Estimation of a signal received in white Gaussian noise using minimization of mean square error is equivalent to maximum likelihood estimation.

Thus a solution will be chosen which is closest, in the mean square sense, to the hypothetical noise-free solution, and yields a "smooth" distribution of amplitudes. Smoothness here is synonymous with stability.

4.1.3 Reduction to Linear System of Equations

Minimization of the likelihood function in (4.5) leads to a linear system of equations:

$$\mathbf{M_0}\, a = \mathbf{d} \tag{4.7}$$

$\mathbf{M_0}$	:	system matrix
a	:	(unknown) amplitudes of the distribution function
$\mathbf{d}$	:	"data" vector (processed)

The inversion problem is hence simplified to a form involving a symmetric, positive definite, invertible (see [7]) kernel matrix $\mathbf{M_0}$, defined by

$$[M_0]_{l,k} = \sum_{m=1}^{N_w} \frac{f_k F_m(T_{2,k}) f_l F_m(T_{2,l})}{\hat{\sigma}_m^2} \tag{4.8}$$

and a data vector $\mathbf{d}$

$$d_l = \sum_{m=1}^{N_w} \frac{\tilde{I}_m f_l F_m(T_{2,l})}{\hat{\sigma}_m^2}. \tag{4.9}$$

$\mathbf{M}$ is a square matrix, whose dimensions N_s are the number of exponential components in the model

$$[\mathbf{M_0}]_{l,k} \in R^{N_s \times N_s} \tag{4.10}$$

The regularized solution, obtained by minimizing (4.6) would yield a similar set of linear equations:

$$\mathbf{M}\, a = \mathbf{d} \tag{4.11}$$

The regularized kernel matrix is related to the non-regularized matrix by a simple boosting of its diagonal elements:

$$\mathbf{M} = \mathbf{M_0} + \gamma \mathbf{I} \tag{4.12}$$

where $\mathbf{I}$ is the identity matrix.

4.2 Eigenanalysis

Reducing the basic inversion problem to a form involving a symmetric kernel matrix allows study of the eigenfunctions of the simplified system. In particular, we are interested in the nature of the eigenfunctions of the system matrix. They define the types of solutions which can be expressed as linear combinations of these eigenfunctions, weighted appropriately. The rank of the system matrix in fact reveals the subset eigenfunctions which contains all the information necessary to derive a solution.

4.2.1 Rank of Kernel Matrix

The real, symmetric matrix $\mathbf{M_0}$ can be diagonalized in terms of an orthonormal set of eigenvectors and corresponding eigenvalues:

$$\mathbf{M_0} = \mathbf{U}\,\mathbf{\Lambda}\,\mathbf{U}^{-1} = \mathbf{U}\,\mathbf{\Lambda}\,\mathbf{U}^{T} \tag{4.13}$$

where the orthonormality of eigenvectors has been exploited to obtain $\mathbf{U}^T = \mathbf{U}^{-1}$. The matrix $\mathbf{U}$ is composed of the eigenvectors $\mathbf{u_1}, \mathbf{u_2}, \ldots, \mathbf{u_i}$ in columns, and the matrix $\mathbf{\Lambda}$ contains the ordered eigenvalues $\lambda_1 > \lambda_2 > \ldots > \lambda_i$ along its diagonal.

$$\mathbf{U} = \begin{pmatrix} \mathbf{u_1} & \mathbf{u_2} & \cdots & \mathbf{u_i} \\ \vdots & \vdots & & \vdots \end{pmatrix} \tag{4.14}$$

$$\mathbf{\Lambda} = \begin{pmatrix} \lambda_1 & & & \\ & \lambda_2 & & \\ & & \ddots & \\ & & & \lambda_i \end{pmatrix} \tag{4.15}$$

Decomposition of $\mathbf{M_0}$ reveals that only a handful of the eigenvalues are non-zero. The matrix $\mathbf{M_0}$ is said to be of finite rank r, where r is the number of non-zero eigenvalues. The solution lies in a finite eigenspace, that is, the space spanned by the r non-zero eigenvalues given in table 4.1 for several choices of windows.

index	*eigenvalues for 5 windows*	*eigenvalues for 10 windows*	*eigenvalues for 15 windows*
1	4737	4810	4814
2	336	351	354
3	40	50.8	51.6
4	4.2	8.5	8.7
5	0.10	1.2	1.3
6		0.15	0.16
7		0.01	0.02
8		0.001	0.001
9		0.000	0.000
10			0.000
11			0.000
12			0.000
13			0.000
14			0.000
15			0.000

Table 4.1: Eigenvalues of System Kernel for Sets of 5, 10, 15 Windows

The eigenvalues and eigenvectors corresponding to table 4.1 for the case of 5 windows and 50 components in the relaxational model ($N_s = 50$) are shown in figure 4-2. Notice that the largest eigenvalue corresponds to the lowest frequency eigenvector; they comprise the slowly varying portion of the solution. The smallest eigenvalue corresponds to the highest frequency eigenvector and allows oscillation in the solution. The solution, then, is comprised of properly weighted eigenfunctions of the measurement kernel. In effect, the solution is described as projections onto a finite set of eigensolutions.

Similar observations can be made for the other cases using more windows. In general, the number of non-zero eigenvalues is determined by the number of superechoes (windows chosen in the data compression scheme) up to a point. In other words, the reduced data set contains all the information that can be extracted from the complete data set. However, adding more windows beyond a certain number does not increase the amount of information that can be retrieved. For the case of 15 windows, note that there are still only a handful of significant eigenvalues. The

magnitude of the eigenvalues drops off very quickly, and beyond the eighth term, they are effectively zero (up to 3 decimal places).

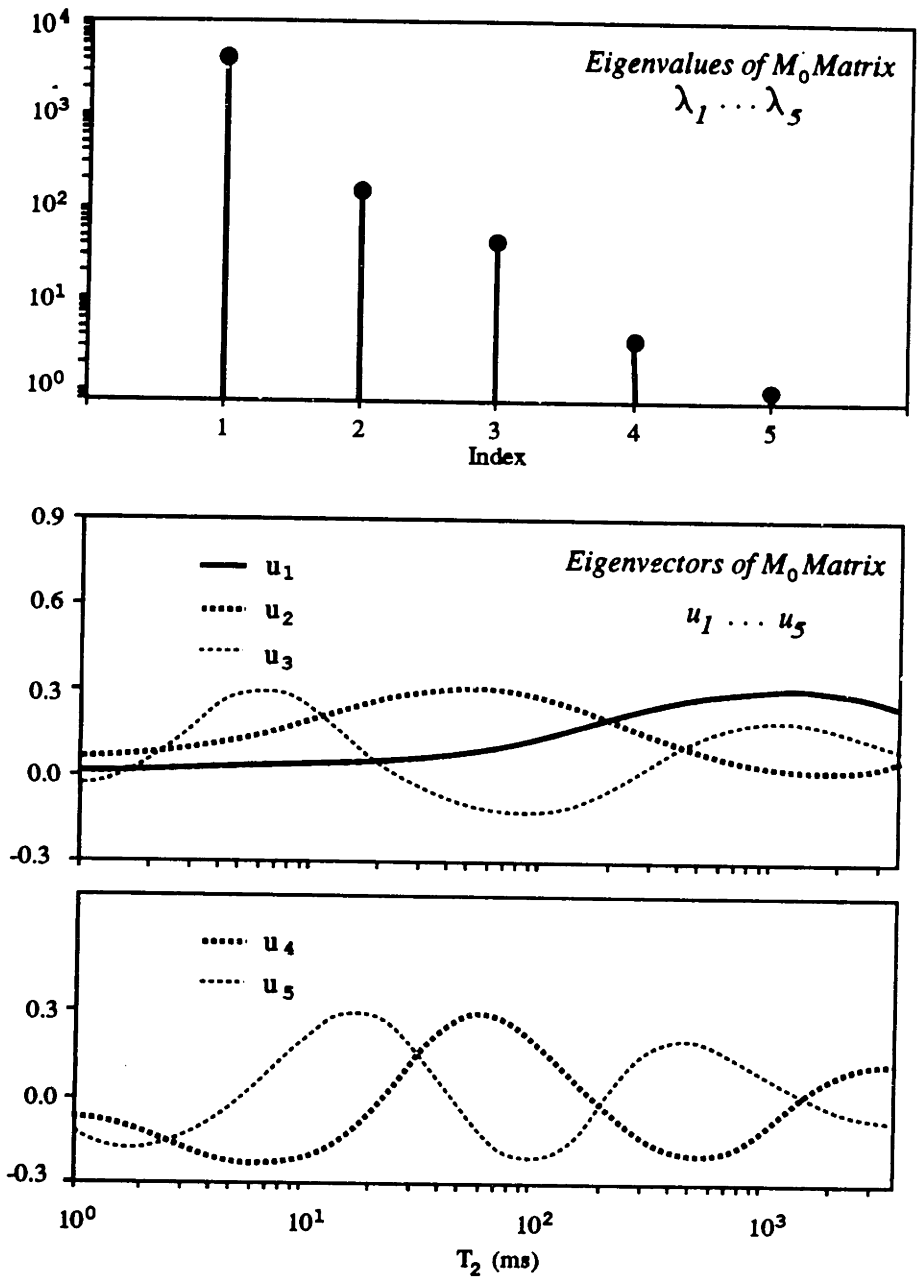

Figure 4-2. Eigenvalues and eigenvectors of system matrix M_0

What is particularly interesting about the cases involving more windows is the corresponding eigenvectors. As the vectors are studied in order of decreasing eigenvalues, they exhibit highly oscillatory behavior. The eigenvectors corresponding to the smallest eigenvalues (for example, the last three in the case of 15 windows) have no visible pattern and display erratic behavior. The solution, which should be smooth, cannot be formulated in terms of these nullspace eigenfunctions.

4.2.2 Expansion in terms of eigenvectors

We begin with our basic equation in matrix form:

$$\mathbf{M_0}\, a = \mathbf{d} \tag{4.16}$$

The eigenvalue decomposition of $\mathbf{M_0}$ leads to:

$$\mathbf{U}\,\mathbf{\Lambda}\,\mathbf{U^T}\, a = \mathbf{d} \tag{4.17}$$

By defining a vector $\mathbf{Q}$ whose components are the projection of the eigenvectors onto the data,

$$Q_i \triangleq \mathbf{u_i} \cdot \mathbf{d} \tag{4.18}$$

a simple solution in the non-nullspace results:

$$a = \sum_{i=1}^{r} \frac{Q_i\, \mathbf{u_i}}{\lambda_i} \tag{4.19}$$

It becomes evident why small eigenvalues lead to instability in the formal solution. Small changes in the data (namely Q_i) lead to large changes in the solution ($\vec{a}$).

4.2.3 Limitations

One of the most obvious limitations of the eigenfunction expansion is that there is no elegant way to constrain the amplitudes to be non-negative. The simplest solution, and the one implemented, is to clip any amplitudes which are negative. In most

cases, the difference in the resulting porosity estimates is negligible. The solution only oscillates slightly at the edges, and the magnitude of the negative terms is minimal.

4.3 Stabilization of Solutions

Baker, Fox, Mayers, and Wright[2] suggested formulating the solution in terms of the dominant eigenvalues of the kernel. Including only the dominant eigenvalues in the expansion in effect filters the solution of high-frequency oscillations, producing more stable solutions than a direct inversion. We will also investigate stabilization via Tikhonov's regularization method; this solution will permit inclusion of all non-zero eigensolutions. We will compare solutions which result from both these approaches.

4.3.1 Dominant Eigenvalues

Since oscillatory behavior of higher-order eigenvectors is associated with the smallest eigenvalues, we consider limiting the expansion to include only the dominant eigenvalues $\lambda_1, \ldots, \lambda_p$.

$$a = \sum_{i=1}^{p} \frac{Q_i \mathbf{u}_i}{\lambda_i} \quad , \quad p \leq r \tag{4.20}$$

In cases where the data is relatively good, meaning with high SNR, it is possible to carry the summation out to p=r. All eigenvectors can be included without fear of instability. However, this is true only for lab or station borehole data, where stacking significantly reduces the noise.

For continuous log data, the SNR is poor, and stability is a real problem. Terminating the summation to include only the dominant eigensolutions filters out high-frequency content; it is up to the user to determine where the cut-off should be. While this approach may be suitable in some situations, filtering out all high-frequency content is likely to produce solutions that are too smooth.

4.3.2 Tikhonov Regularization

Here we make use of the regularized kernel matrix M from 4.12, whose diagonal elements have been boosted by the regularization constant γ. Adding a regularization term allows use of all non-zero eigenvalues and associated eigenvectors in the solution, even in cases where SNR is very low. The following solution results for a:

$$a = \sum_{i=1}^{r} \frac{Q_i \mathbf{u}_i}{\lambda_i + \gamma} \tag{4.21}$$

The regularization parameter simply augments the eigenvalues λ_i and has the pleasing effect of dampening out oscillatory behavior.

4.4 Optimal Regularization

We now treat a general strategy for choosing the regularization parameter as a function of the error level present in the data. Although many forms of regularization have been suggested in past literature, the form chosen in this study, primarily for reasons of simplicity in implementation, was the L_2 norm. Once this was established, we wished to study a means of selecting an optimal value of the regularization parameter. Work due to Butler, Reeds, and Dawson [4] formed the basis for an optimality criterion. A revised form of the BRD criterion was later implemented which is better tailored for this application.

4.4.1 Butler-Reeds-Dawson Optimality Criterion

A criterion for optimality was chosen to be the solution which minimizes the error between the regularized solution and a hypothetical noise-free solution. Let a denote the regularized solution given by an eigenfunction expansion in the non-nullspace:

$$a = \sum_{i=1}^{r} \frac{Q_i \mathbf{u}_i}{\lambda_i + \gamma} \tag{4.22}$$

Let a_0 be a hypothetical solution, derived from the multi-exponential model, in the absence of noise (notice the hypothetical solution has no need for regularization):

$$a_0 = \sum_{i=1}^{r} \frac{(Q_0)_i \mathbf{u_i}}{\lambda_i} \tag{4.23}$$

A vector $\mathbf{Q_0}$ has been defined, whose components are the projections of the eigenvectors onto the "noise-free data."

$$(Q_0)_i \triangleq \mathbf{u_i} \cdot \mathbf{d_0} \tag{4.24}$$

$$\mathbf{d_0} = \mathbf{d} - \mathbf{n} \tag{4.25}$$

where $\mathbf{n}$ is the noise:

$$n_l = \sum_{m=1}^{N_w} \frac{\tilde{N}_m f_l F_m(T_{2,l})}{\hat{\sigma}_m^2} \tag{4.26}$$

and $\tilde{N}_m$ is defined as the sum of the noise across the m^{th} window.

Following Butler-Reeds-Dawson, we define a solution error:

$$F_\gamma = \| a - a_0 \|^2 \tag{4.27}$$

Obviously it is impossible to solve for a_0 since the distribution is unknown. We must assume something about the nature of the expected solution in order to solve (4.27). We will assume that the data is co-linear with the noise, an assumption also made by Butler, Reeds, and Dawson:

$$\mathbf{Q} = s\,\mathbf{Q_0} \tag{4.28}$$

s is defined by

$$s = \sqrt{\frac{< \mathbf{Q_0^T Q_0} >}{< \mathbf{Q^T Q} >}} \tag{4.29}$$

The optimal choice for the regularization parameter γ_{opt} is one for which the solution error is minimized. Solving for the minimum of (4.27) and making use of the assumption in (4.28) yields a transcendental equation to be solved for the optimum

value of γ:

$$\gamma = \frac{s}{1-s} \frac{\sum_{i=1}^{r} \frac{Q_i^2}{(\lambda_i+\gamma)^3}}{\sum_{i=1}^{r} \frac{Q_i^2}{\lambda_i(\lambda_i+\gamma)^3}} \tag{4.30}$$

It can be shown that there are bounds on γ_{opt}, and that a solution will always exist between the bounds:

$$\frac{s}{1-s}\lambda_r \leq \gamma_{opt} \leq \frac{s}{1-s}\lambda_1 \tag{4.31}$$

provided s < 1.

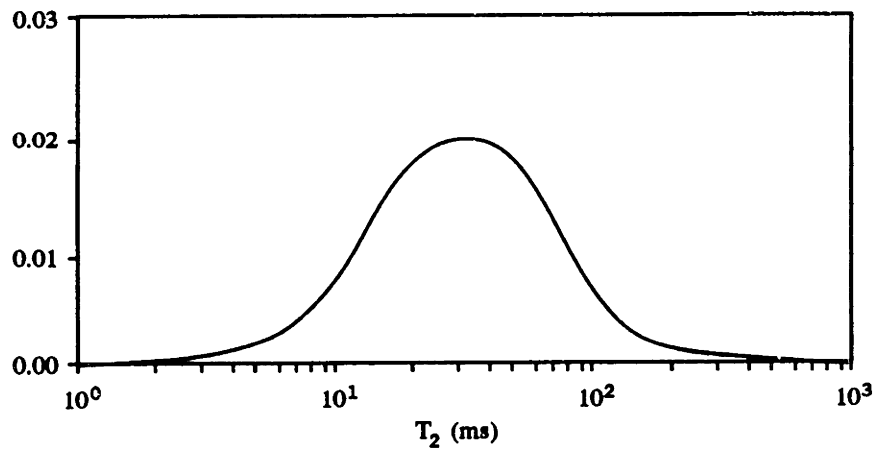

Figure 4-3. Gaussian distribution used to generate syntethic data

To study the nature of the BRD function, an input Gaussian distribution (see figure 4-3) was used to generate synthetic CPMG data with random additive noise. Estimates were derived for a wide range of γ to study the behavior of the solution error with respect to γ. Plots of the BRD function F_γ for 10% and 20% noise levels are included in figure 4-4.

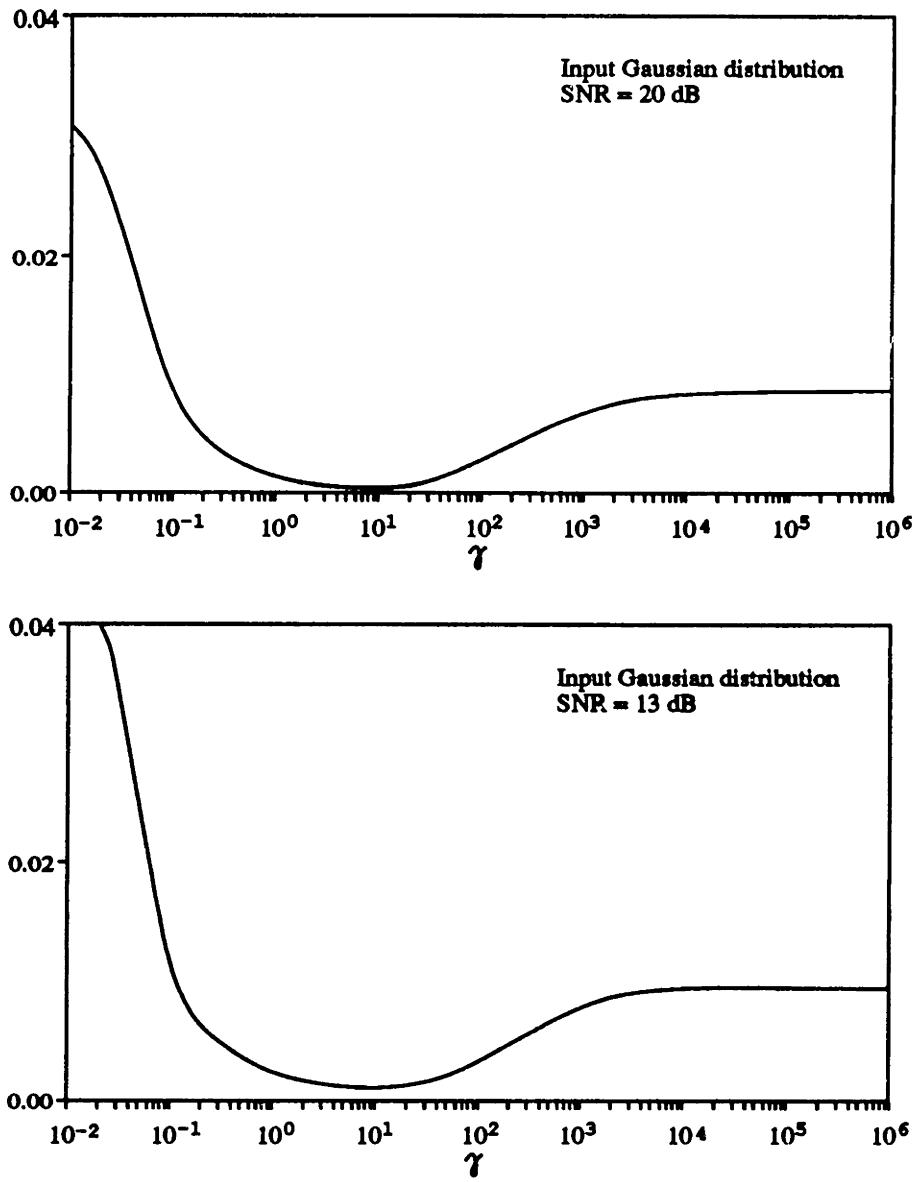

Figure 4-4. Illustrations of the BRD function vs.γ

Some qualitative observations can be made which seem to hold generally. The solution error becomes increasingly large for small values of γ as the noise level is increased. This observation is reasonable since higher noise levels will yield more spurious solutions in the absence of regularization, or using minimal regularization. For a given data set, Very high values of γ over-regularize the distribution, and the solution error approaches a constant as γ is increased. If γ is very small, the error also increases. This agrees with Twomey's results [23]. For either very small or very large values of γ, solutions will not be close, in the mean square sense, to the hypothetical noise-free solution.

Between these two extremes lies the minimum, or the optimum value of γ. Notice that the function is fairly flat in this region, illustrating that it is not particularly sensitive to the actual value of γ. Experimentation with actual inversions has agreed closely with this observation. The answer products, and even the distribution itself, do not change considerably for a range of "optimal" γ values.

In the presence of random error, the residual is fairly flat for a region when plotted against γ. In this region, the residual is somewhat independent of the particular choice of γ.

4.4.2 Revised Optimality Criterion

A revised optimality criterion still mandates that the distribution be closest, in the mean square sense, to the hypothetical solution. In addition, it ensures that the porosity estimates derived from the distribution, be optimized with respect to the hypothetical porosity estimates. It is obtained by minimization with respect to γ of the function:

$$F_\gamma = \| a - a_0 \|^2 + \beta \| \phi - \phi_0 \|^2 \tag{4.32}$$

The porosity estimates are simply related to the distribution function of amplitudes originally sought:

$$\phi = K_{tool} \sum_{l=1}^{N_s} a_l \tag{4.33}$$

$$\phi_0 = K_{tool} \sum_{l=1}^{N_s} (a_0)_l \tag{4.34}$$

The constant β can be chosen to suit a particular application, and is particularly useful in reducing variance in porosity estimates. For "good" data, it is possible to accurately estimate a distribution function, and β would be set to zero. For noisier data, however, it is nearly impossible to estimate a distribution with any degree of success. In such cases a relatively high value of β would be used to boost the priority of selecting a solution which minimizes the variance in the porosity estimation, at the expense of detail (and accuracy) in the resulting distribution.

A similar minimization of (4.32) again leads to an equation which can be solved for an "optimal" γ.

$$\gamma = \frac{s}{1-s} \left[\frac{\sum \frac{Q_i^2}{(\lambda_i+\gamma)^3} + \beta \sum \frac{Q_i v_i}{(\lambda_i+\gamma)^2} \sum \frac{Q_i v_i}{\lambda_i+\gamma}}{\sum \frac{Q_i^2}{\lambda_i(\lambda_i+\gamma)^3} + \beta \sum \frac{Q_i v_i}{(\lambda_i+\gamma)^2} \sum \frac{Q_i v_i}{\lambda_i(\lambda_i+\gamma)}} \right] \tag{4.35}$$

where the summations range from $i = 1, \ldots, r$. The scalars v_i are the sums of the components in each eigenvector:

$$v_i \equiv \sum_{j=1}^{N_s} \mathbf{u}_{ij} \tag{4.36}$$

The notation $\mathbf{u}_{ij}$ refers to the j^{th} component of the i^{th} eigenvector.

Figure 4-5 shows the revised BRD condition as a function of γ. The minimum is sharpened, and the peak has been shifted to larger values of γ. We have added additional constraints to the optimality criterion, and fewer values of γ will satisfy the new minimum error condition.

Figure 4-6 shows our results for the automatic selection of γ for various levels of rms noise. As expected, the noisier the data, the more smoothing is employed. Our newest parameter in the algorithm, β provides a mechanism for securing even smoother, and hence more stable, solutions.

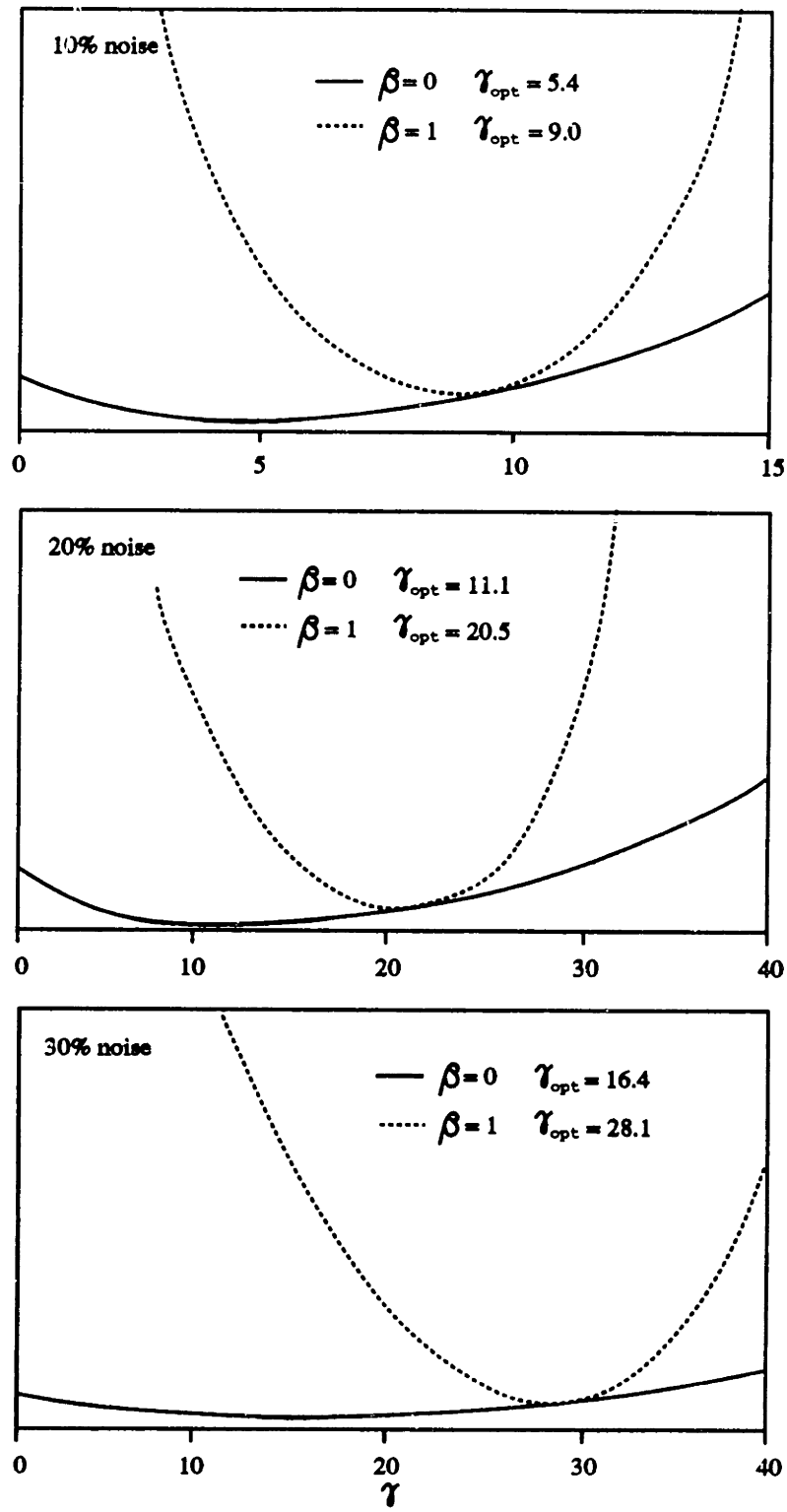

Figure 4-5. Illustrations of the revised BRD function vs.γ

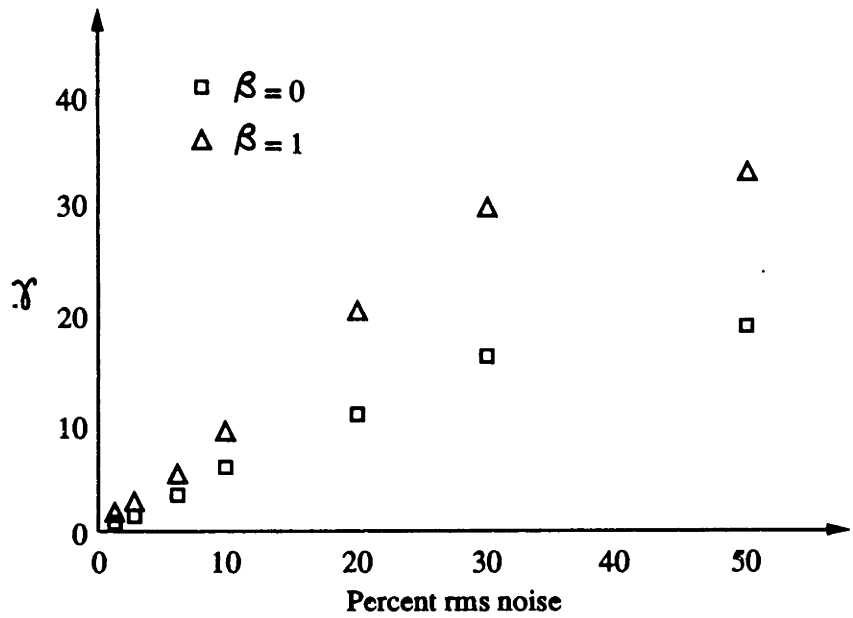

Figure 4-6. Automatic selection of regularization parameter

4.4.3 Variable Regularization

All previous discussions and derivations have assumed a constant regularization parameter γ. In the course of the study, advantages of allowing a function instead of a constant regularization term were considered.

Firstly, we investigated the possibility of using two regularization terms, γ_{bf} and γ_{ff}, to reflect the distinction between slow and fast relaxation rates. It was hypothesized that γ_{bf} would in general be less than γ_{ff} since the components during the fast decay should not be over-regularized. However, testing showed that it was wrong to consider an abrupt case of simply two values for γ in the two regions. Results for this case, using two regularization constants, are presented in the next chapter.

Based on the failure of discontinuous values for γ, we further investigated the merits of using a continuously varying $\gamma(T_2)$. It turns out that the solutions obtained using a function for γ were fairly accurate, but the solutions using a simple constant regularization term were also comparable. This result agrees with our previous ex-

amination of the BRD function, which revealed that the error in our estimates is not strictly dependent on γ. For simplicity, then, we decided to continue our study using a constant regularization parameter.

A flowchart outlining the steps in our inversion algorithm is given in figure 4-7.

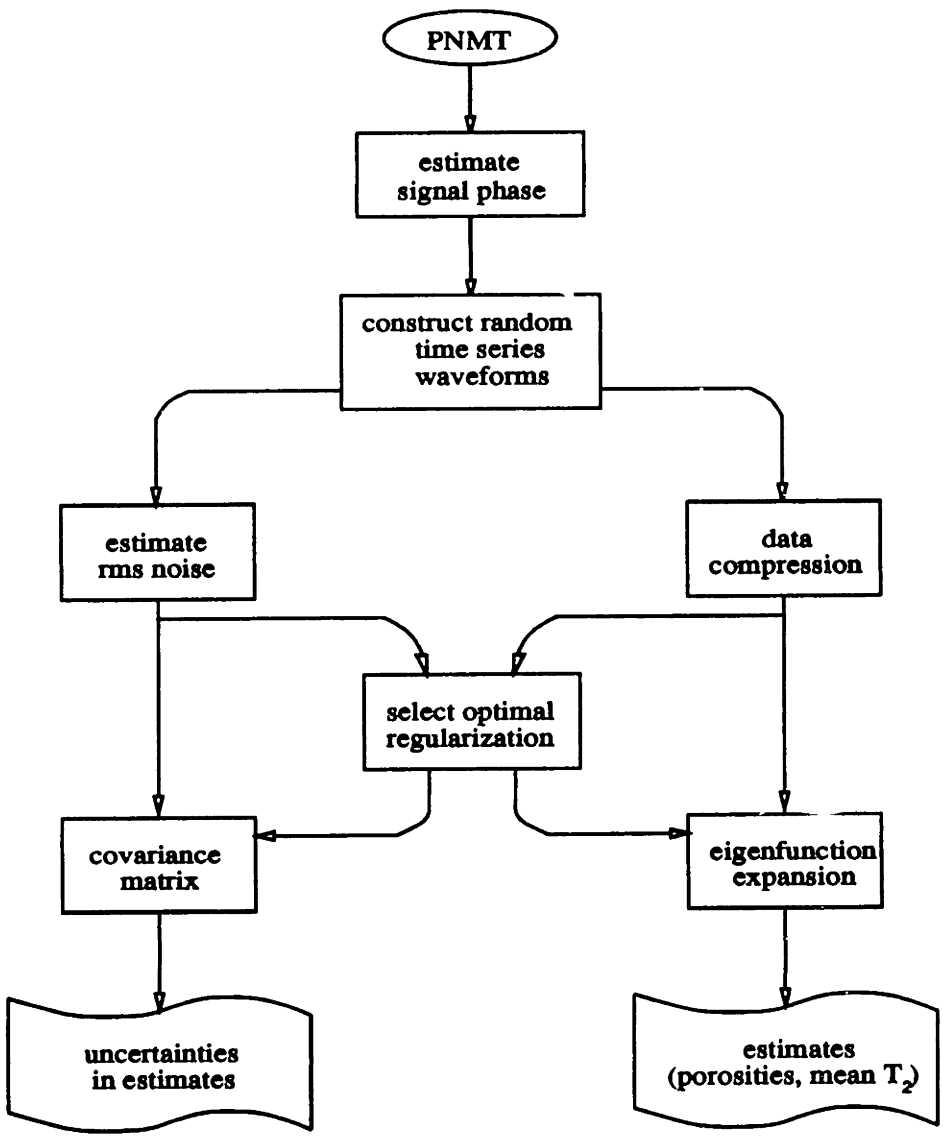

Figure 4-7. Flowchart of the inversion algorithm

Chapter 5

Simulations

5.1 Distributions and Answer Products Obtained from Inversion

We will examine the distributions of relaxation time obtained from the eigenfunction expansion analysis. The distributions can be used to determine the final answer products ϕ_{nmr}, ϕ_{ff}, and $\bar{T}_{2,log}$. The porosities are weighted integrals of the distribution function. $\bar{T}_{2,log}$ is the logarithmic mean of the decay time distribution. The answer products are defined as follows:

$$\phi_{nmr} = K_{tool} \sum_{i=1}^{N_s} a_l \tag{5.1a}$$

$$\phi_{ff} = K_{tool} \sum_{i=1}^{N_c} a_l \tag{5.1b}$$

$$\bar{T}_{2,log} = 10 \exp\left(\frac{\sum a_l \, log T_{2,l}}{\sum a_l}\right) \tag{5.1c}$$

In many cases, the accuracy of the answer products derived from the distributions are more important than the actual signal distributions obtained.

5.2 Inversion of Synthetic Data

5.2.1 Results using Dominant Eigensolutions

The method of including only dominant eigenfunction in the expansion does not need formal regularization. Exclusion of high-frequency terms is a form of filtering, and smooth solutions are obtained automatically. We illustrate the effect of including additional terms in the expansion, that is, eigenvectors other than those corresponding to the dominant eigenvalues, in figure 5-1. The solution represented by the solid line (corresponding to the dominant 3 eigenvectors) resembles the input Gaussian distribution. Notice the smoothness obtained by restricting the expansion to the dominant 3 eigenfunctions. The solution represented by the dotted line is obtained by extending the expansion out to the fourth largest eigenvector (total of 5 eigenvalues and eigenvectors were available for the choice of 5 windows).

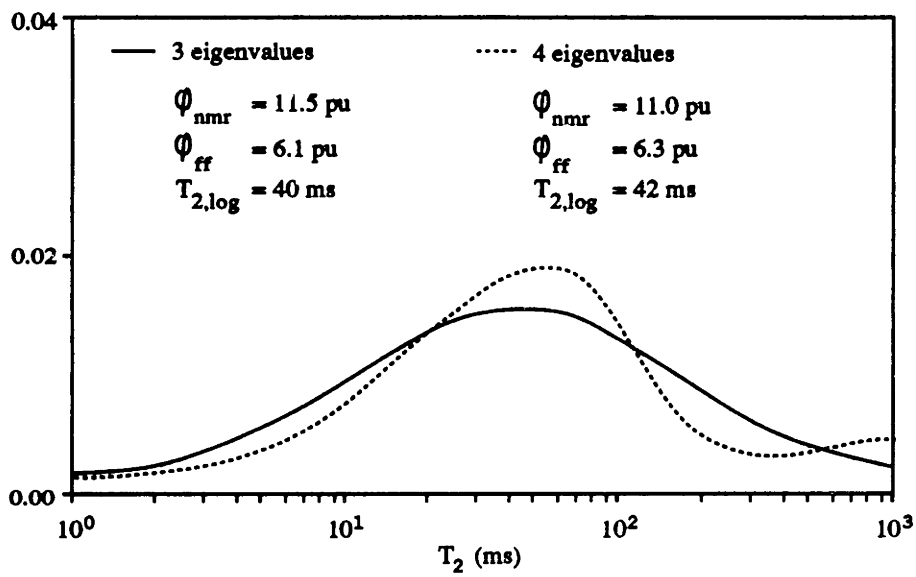

Figure 5-1. Estimated distributions using dominant eigenvectors (5 windows)

From this experiment it seems that, if we wish to use the dominant eigenvalues method, three eigenvectors are sufficient to represent the solutions. That is to say, the rank of our system matrix is 3. We further tested our theory by changing the data compression portion to use 10 windows instead of 5. Figure 5-2 shows the solutions obtained for expansions including 3, 4, and 5 dominant eigenvectors.

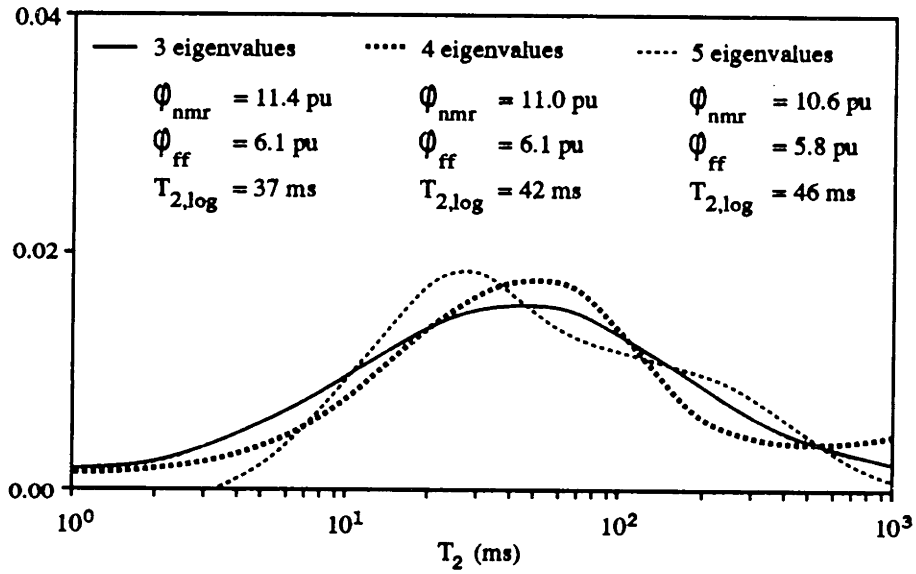

Figure 5-2. Estimated distributions using dominant eigenvalues (10 windows)

Notice that the case resulting from using 3 eigenfunctions (out of 10) is remarkably similar to that of using 3 out of 5 from the previous example. Thus we concluded that, for PNMT data with SNR $\approx$ 20–25 dB, carrying the eigenfunction expansion out to the third largest eigenfunction will yield good results. Including any terms beyond that will result in oscillatory behavior that is not consistent with our model of relaxation times and the smooth measurement kernel.

5.2.2 Variable Regularization

Early in our study we investigated the solutions obtained by using two values of the regularization parameter to reflect the difference in our estimates for free-fluid and bound-fluid porosities. Eager to see if this slight modification of our formal derivation for a single constant γ would improve our estimates, we tested the case of a simple Gaussian input distribution. In retrospect, it is obvious that this selection of distinct terms for the two regions will not yield a favorable distribution; the abruptness in the regularization term does not conform to the desired smooth distribution function. Figure 5-3 shows the discontinuity in the resulting solution.

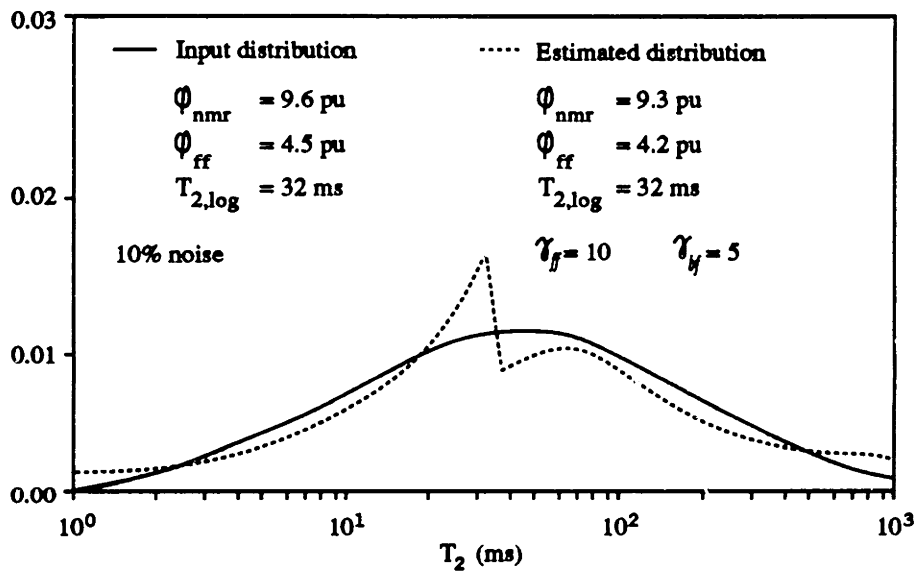

Figure 5-3. Solution using two discrete regularization terms

We next revised our algorithm to utilize a smooth function of γ, where the transition between γ_{ff} and γ_{bf} was a smooth, non-linear one. This version was significantly more complex, since at each step a different value of γ was used. Figure 5-4 shows the result obtained for regularization effected by a function for γ.

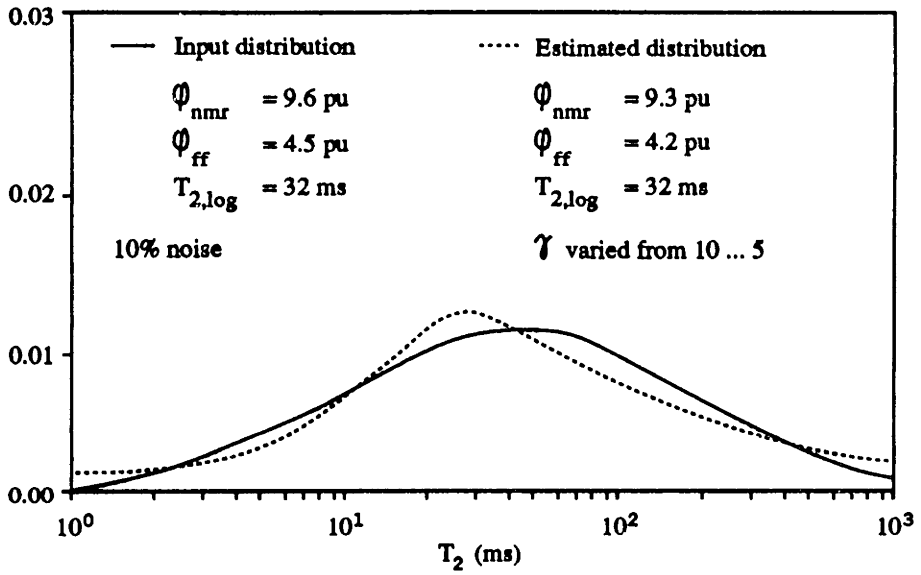

Figure 5-4. Solution using variable γ

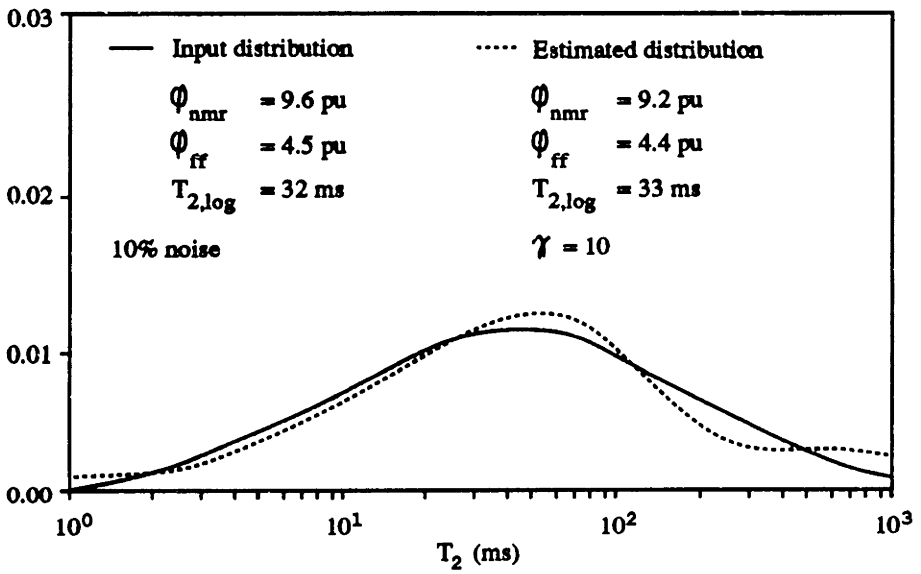

Figure 5-5. Solution using constant γ

Although the solutions obtained were fairly accurate, using a function for γ provided no advantage over using a constant γ in terms of both the distributions achieved and final porosity estimates (see figures 5-4 and 5-5). In effect, the distributions are relatively insensitive to the actual value of the regularization parameter. This is consistent with our study of the BRD criterion used to select an "optimal" regularization term. The flat minimum suggested there was a range of values which could perform equally well. Regularization is certainly necessary, but the actual value used can be somewhat flexible.

5.2.3 Mobility of Window Boundaries

The window boundaries chosen in the early stages of pre-processing, in the data compression scheme, are based on results of numerical simulations with a variety of distributions (investigated by Freedman [7]). We were interested in affirming that the algorithm is robust to other choices for window boundaries. We chose two window sets and examined their eigenvectors (see figure 5-6). There are slight differences, as expected, but they are similar in nature and it makes sense that our estimated distributions can be expressed equally well in terms of either set of eigenvectors.

The choice of a set of window boundaries determines our system matrix and its eigenfunctions. Hence different window sets will yield different eigenfunctions, but they are equally valid. Our solution, non-unique as we have stressed throughout, can be expressed in terms of any complete set of non-nullspace eigenfunctions. The weights for each term in the expansion will of course differ to reflect the use of different basis functions. The distributions obtained from expansions in terms of two chosen window sets (two different but equally valid sets of eigenfunctions) are comparable, as shown in figure 5-7.

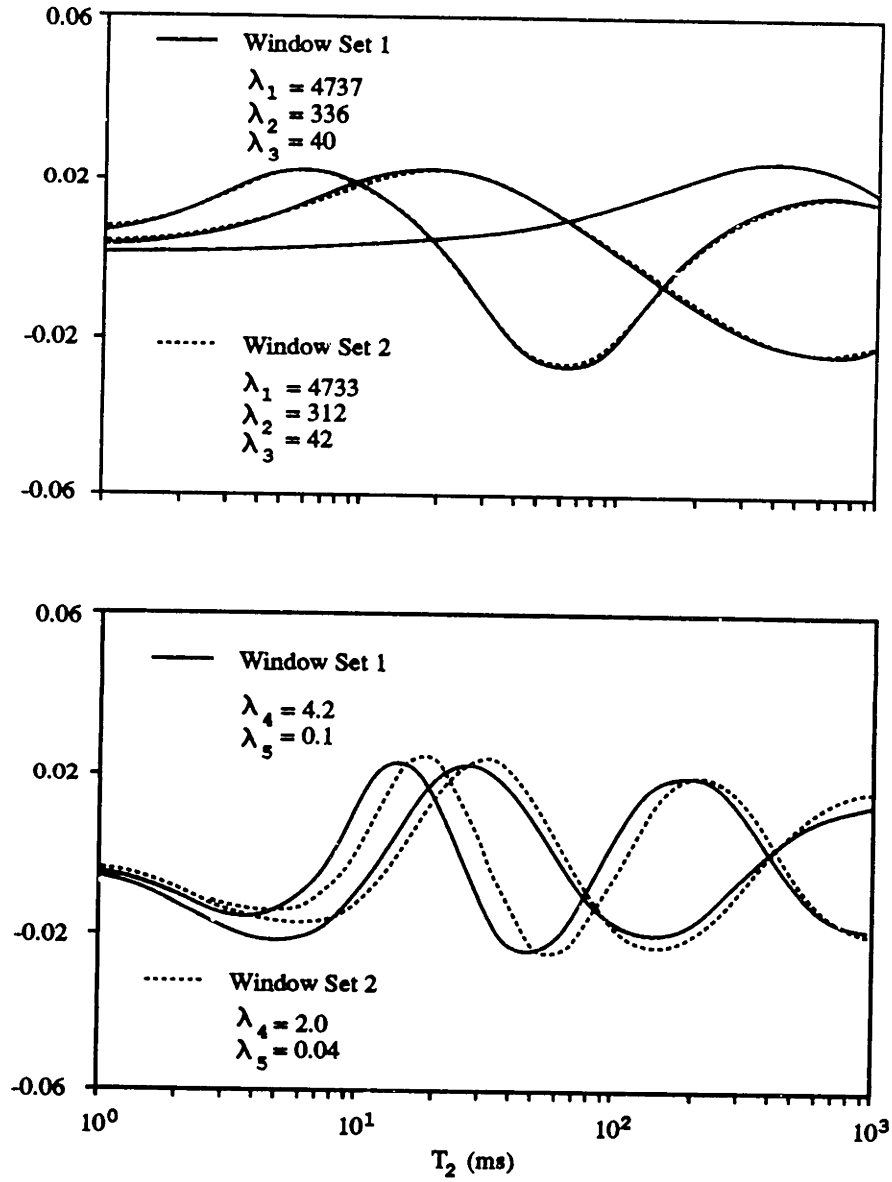

Figure 5-6. Eigenvectors for two sets of window boundaries

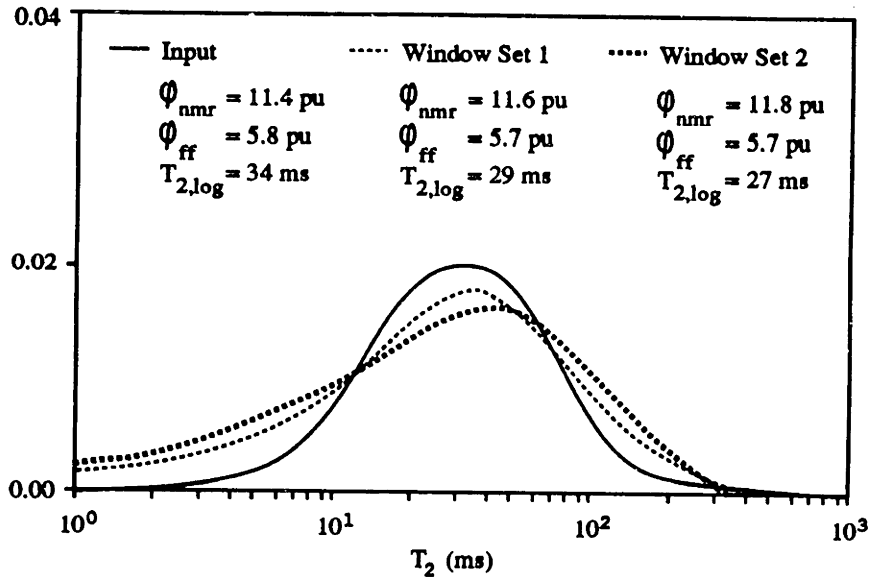

Figure 5-7. Estimated distributions from different window sets

5.2.4 Bimodal Distributions

We also showed that bimodal input distributions are recoverable. Although the exact shape may not be preserved, the resulting porosity and mean relaxation time estimates are still relatively accurate. Figure 5-8 is representative of the types of solutions we obtained. The general bimodal shape is reflected, though it does not agree closely with the actual input distribution, and the final answer products are reasonable.

Note should be taken that our algorithm is capable of inverting bimodal distributions. However, the examples we chose placed heavy weight on the fast decaying components. The algorithm is insensitive to quickly decaying parts in the spectrum, based on the windowing data compression taken. The first window is the only one which reflects quickly decaying components. The slowly decaying components will be reflected in all of the windows, and hence can be recovered most reliably. The fast components are difficult to trace, and hence distributions corresponding to mostly bound-fluid porosity are especially difficult to invert.

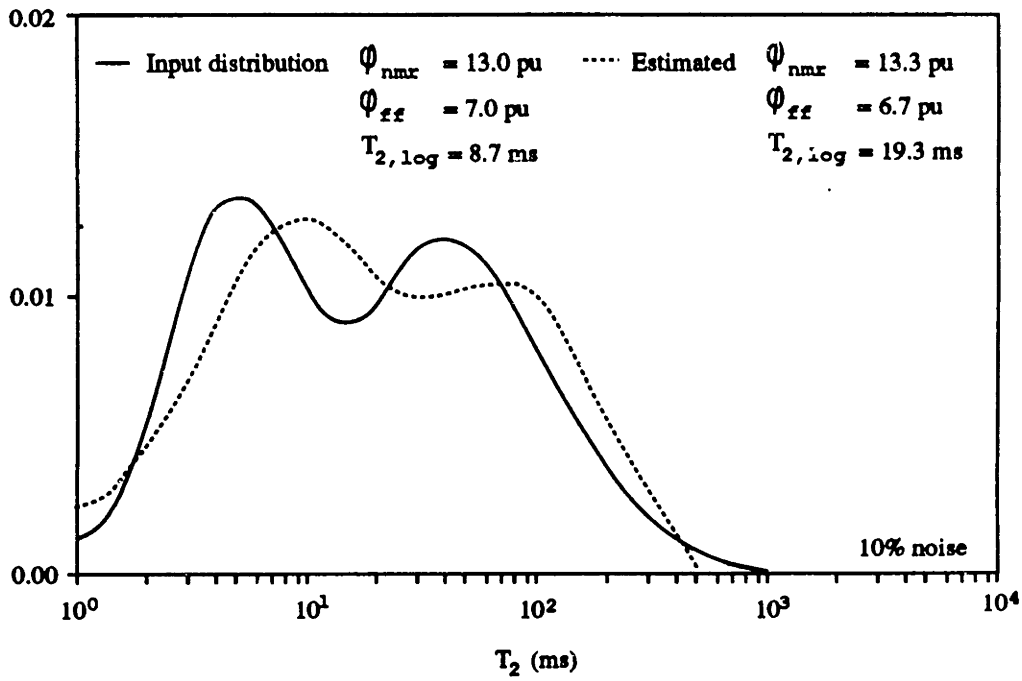

Figure 5-8. Inversion of bimodal distribution

5.3 Monte Carlo Simulations using Real Log Data

When examining real CPMG data, we often are interested simply in the answer products. The high level of noise makes estimation of a detailed distribution function unfeasible, but accurate estimates in porosity and mean relaxation time are still achievable. The integral of the derived distribution, then, is more robust than the distribution itself. We analyzed this process by taking an input Gaussian distribution of relaxation times and generating 100 cases of CPMG data with 35% rms noise added. It is important that the estimates obtained are unbiased and at the same time have the smallest level of variance possible.

Figure 5-9 shows the answer products for 100 trials, where the amplitudes in the "distribution" are clipped if negative. Notice there is a slight bias (overestimation) in the estimates since negative wiggles at the tails of the derived distributions are clipped. Nevertheless, the estimates are quite reasonable. The top graph shows the total porosity (ϕ_{nmr}), the middle graph the free-fluid porosity (ϕ_{ff}), and the bottom graph the logarithmic mean relaxation time ($\bar{T}_{2,log}$). Solid lines indicate the true porosities and mean relaxation time, and sample means and standard deviations are shown as well.

Figure 5-10 differs from the previous case only in that negative amplitudes were allowed. This option, though it violates the fact that amplitudes cannot be negative, yields less biased estimates for the answer products.

We note that, had a larger value of the regularization parameter γ been chosen, the estimates would have less variance, but the bias would be increased. Thus we again see a tradeoff in selection of γ. Clearly both reduced variance and lack of bias are desirable, but favoring one automatically disfavors the other.

We even ran Monte Carlo simulations for cases with 50% rms noise; results are given in figure 5-11. This is the highest level of noise (worst possible case) we expect to see in any logging job. Estimates are good given the high noise level.

For completion, these results were benchmarked against results obtained from existing algorithms, and they proved to be equally valid. The following section further explores the actual distributions obtained from another algorithm. We can then satisfactorily claim that our eigenfunction expansion solution yields results at least as "good" as existing solutions.

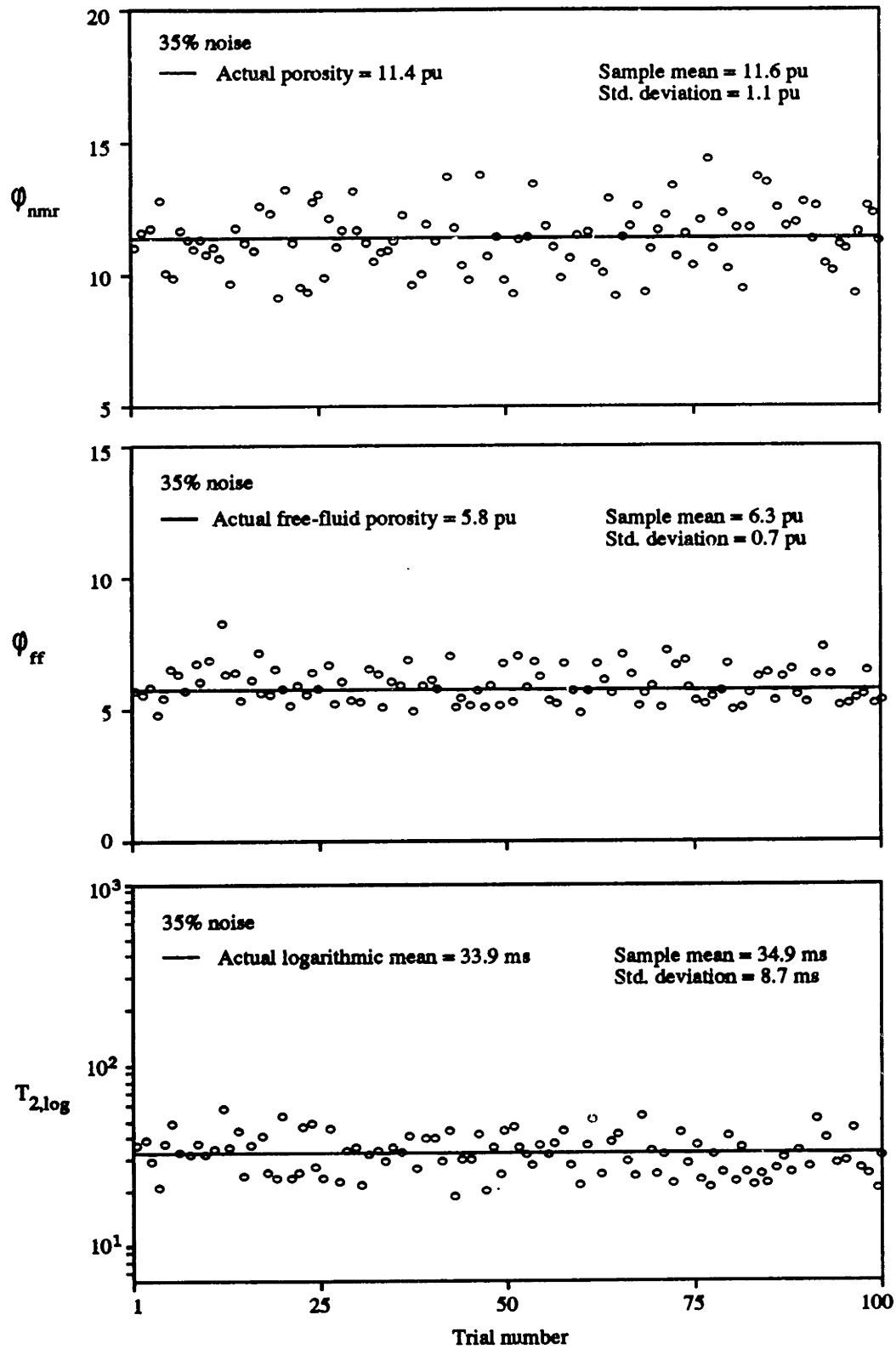

Figure 5-9. Monte Carlo simulations for estimated answer products

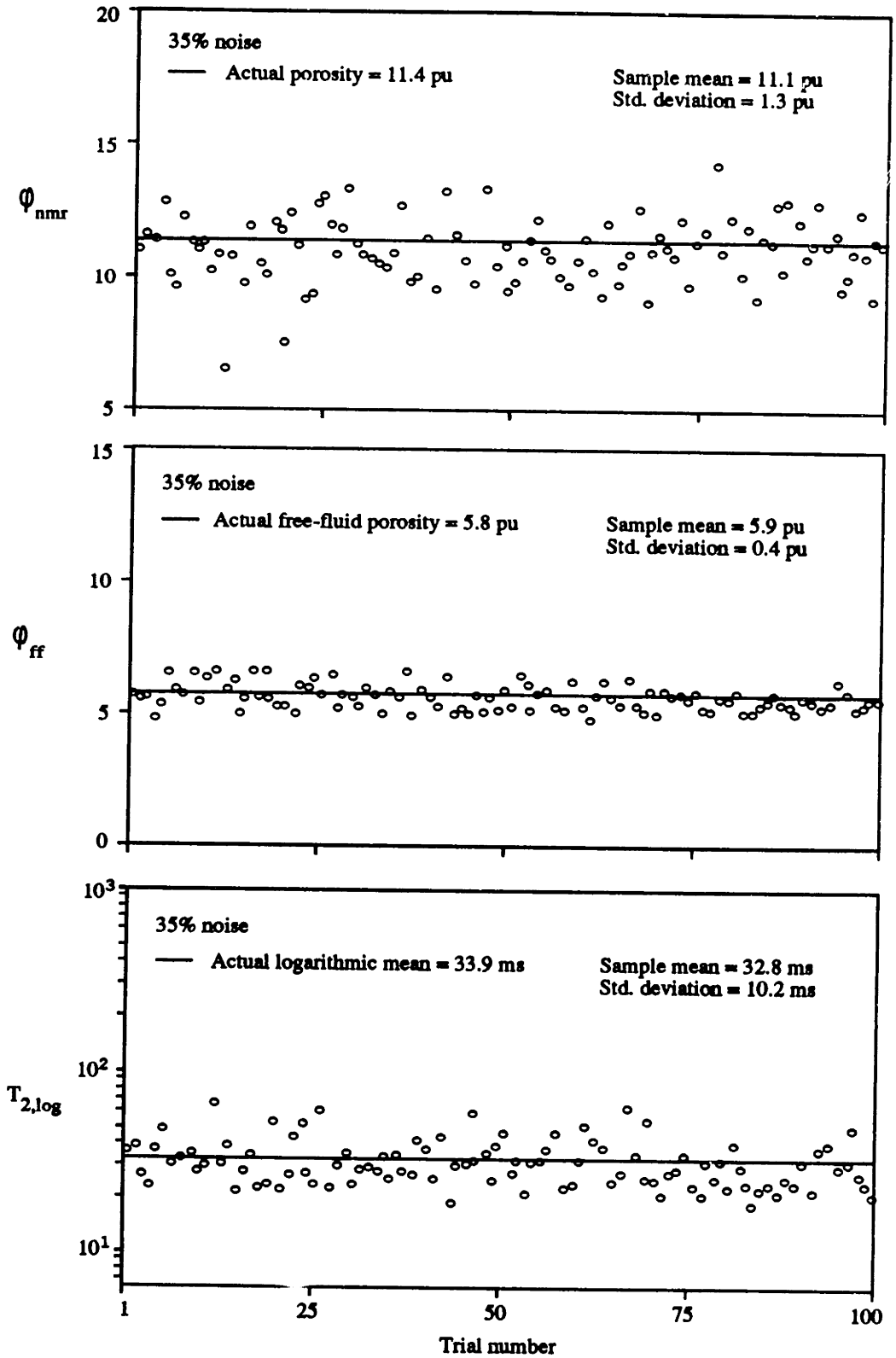

Figure 5-10. Monte Carlo simulations for estimated answer products

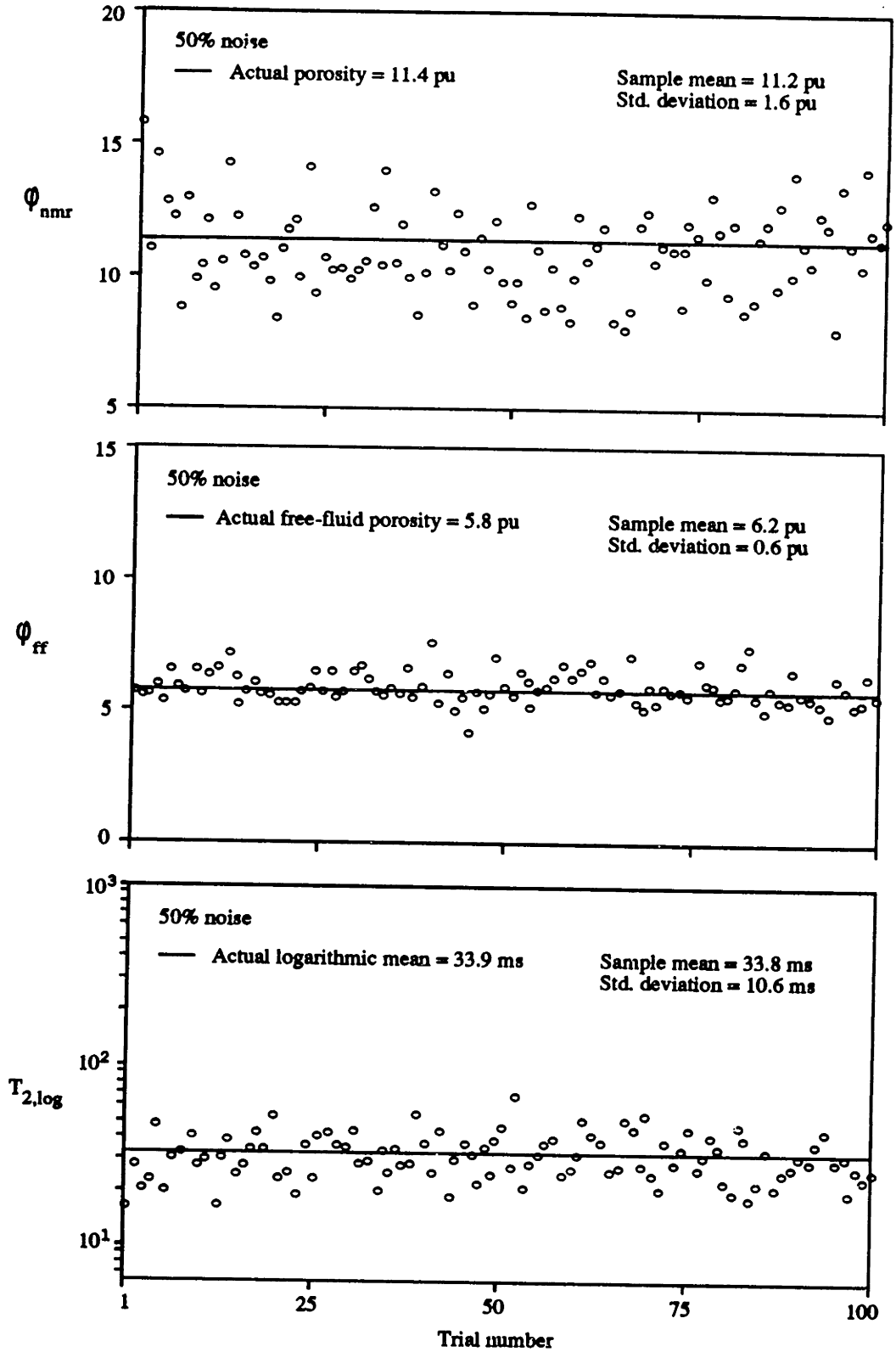

Figure 5-11. Monte Carlo simulations for estimated answer products

5.4 Comparison to Existing Inversion Schemes

Many test cases were compared to ensure that the present algorithm produces results which agree with those from existing inversion schemes. An implementation due to Freedman [7] was used to compare solutions. In all cases we observed close agreement between distributions and porosity estimates obtained from either algorithm. A collection of simulations follows which illustrates the similarities in the final answer products.

Figure 5-12 show comparisons of Freedman's algorithm and our eigenfunction expansion algorithm for the cases of 5%, 10%, and 20% additive random noise. A Gaussian input distribution was chosen for this example, with the peak at a moderate relaxation time. Our estimates are not as successful when the peak rests at faster relaxation times, as illustrated in figure 5-13. As discussed previously, this difficulty arises from the fact that quickly decaying components are especially difficult to trace. Results are better when the distribution does not give such heavy weighting to fast components. Figure 5-14 is comprised of mostly free-fluid porosity, with a hint of a bimodal nature.

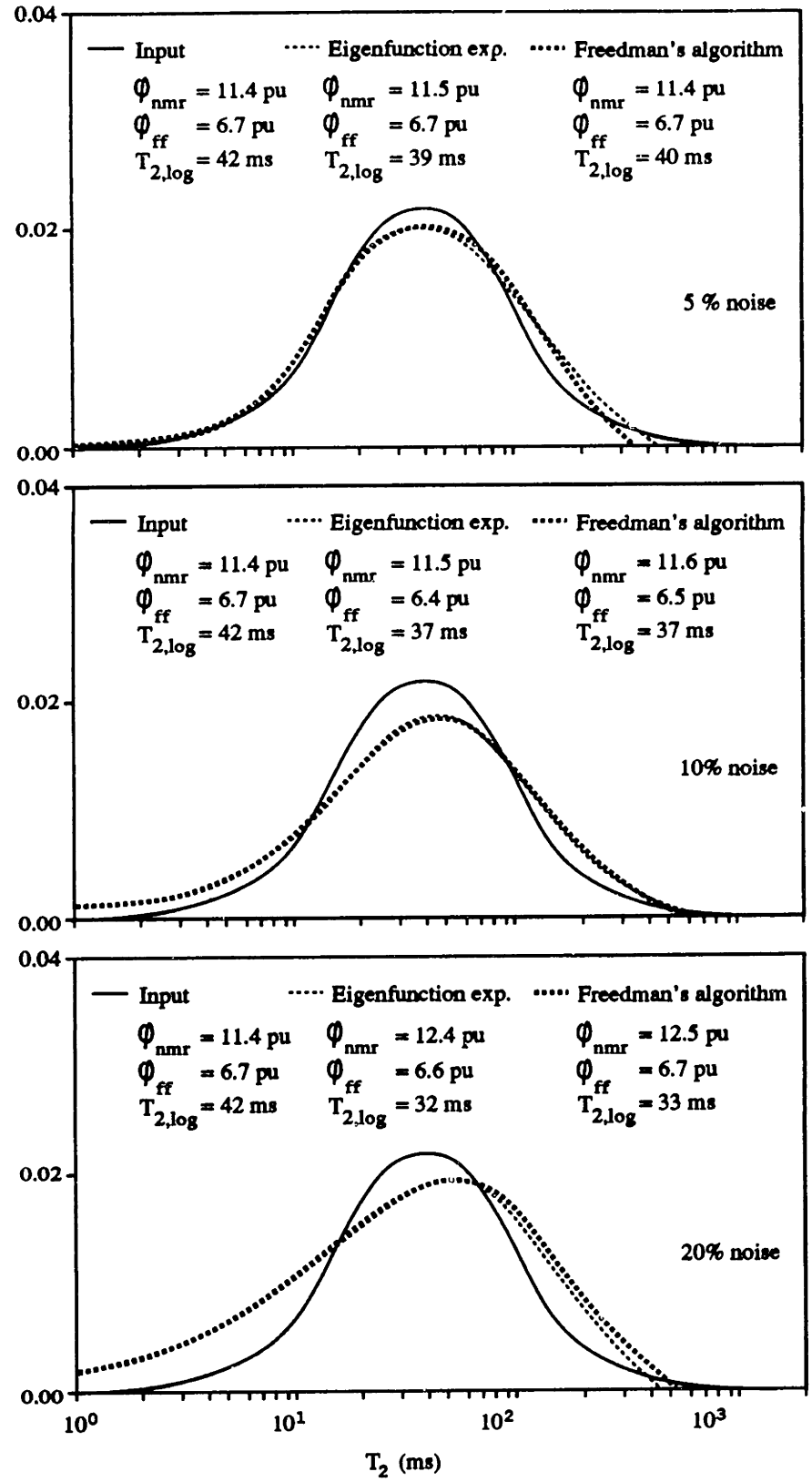

Figure 5-12. Comparison of inversion algorithms for an input distribution with 5%, 10%, and 20% additive random noise

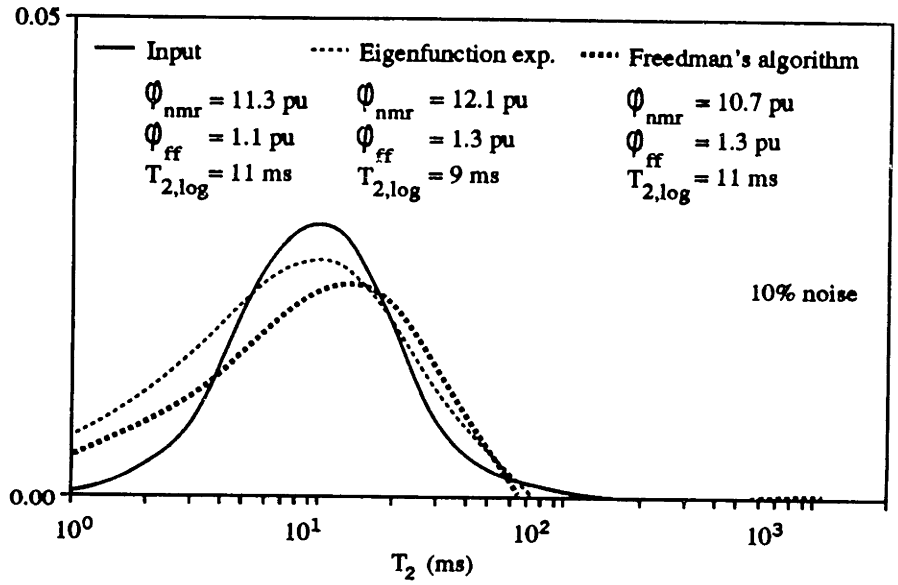

Figure 5-13. Comparison of inversion algorithms for an input distribution of mostly fast relaxation times

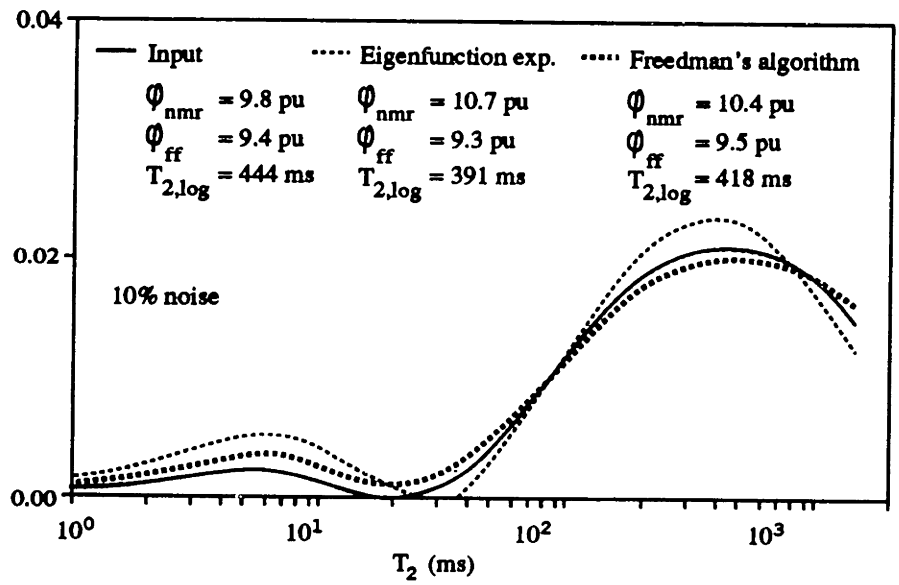

Figure 5-14. Comparison of inversion algorithms for an input distribution of mostly slowly decaying components

Chapter 6

Conclusions

An eigenvalue analysis approach was taken to derive a solution to the inversion problem. The solution was formulated as a linear combination of weighted eigenfunctions. The finite rank of the system matrix revealed that a subset of the eigenfunctions could be used in the solution; the solutions have no projections in the nullspace.

When signal-to-noise ratio is better than $\approx$ 10 dB (such as for station data, where measurements are repeatedly collected and stacked) and the distribution is very smooth, it suffices to carry out the expansion to the eigenvectors corresponding to the dominant eigenvalues only. As long as the noise level is fairly low, the resulting solutions are numerically stable since the high-frequency components have been excluded. When higher noise levels are introduced, however, as in continuous log data, stability becomes a very real issue. Wild oscillations due to noise artifacts are part of the formal solution. The stability issue is addressed via Tikhonov regularization.

Regularization behaves as a filter on the unstable solutions and smooth out oscillatory behavior. Many types of regularization are possible; we chose the simplest form, the L_2 norm, for our application. We next addressed a method for choosing an "optimal" regularization constant. We studied one criterion, the Butler-Reeds-Dawson function, which seeks to minimize the fit error between a hypothetical noise-free solution and the solution dictated by varying choices of γ. When the BRD function was plotted against γ, it become clear the actual value of the regularization constant was not critical. Although regularization is crucial in stabilizing the solutions,

a range of values will perform equally well. The regularization term is chosen in a data-dependent manner: the higher the level of noise present in the data, the higher the value of γ_{opt} chosen.

As γ is reduced, the solutions tend to become more "wavy." One of the real difficulties in inversion work is to decipher when these fluctuations are real and when they are simply artifacts due to noise amplification. Conversely, as γ is increased, the solution becomes over-regularized and no longer depends substantively on the data. Although the variance or uncertainty in the estimates is smaller, a large bias is introduced. This tradeoff between numerical stability and bias in the solution frames the bounds of γ which can be successfully used in the inversion.

We ran a wide variety of simulations to test the robustness of our algorithm and obtained good results. Bimodal and unimodal input distribution were used. We found that broad distributions are easiest to invert, since those exponentials affect all window sums. Distributions with short decay times (mostly bound-fluid porosity), though, are encapsulated mostly in the first few windows and are not as easily recoverable.

The final answer products are weighted integrals of the derived relaxation time distribution. While the exact distribution may not be recoverable when noise levels are high, the answer products need to be dependable. We have demonstrated, through Monte Carlo simulations, that the porosity and mean relaxation time estimates are accurate even when the actual distributions achieved do not match the input distribution very closely. This is of significance when actual log data is processed.

While inversion algorithms exist [7] [17] to process pulsed NMR data from downhole measurements, we approached the problem from a different perspective, namely eigenanalysis. Our solutions agreed closely with those obtained from existing algorithms. The study was useful primarily to learn about the nature of the measurement kernel and its eigenfunctions, which form the basis for the types of solutions we can derive.

Bibliography

[1] A. Abragam. *The Principles of Nuclear Magnetism.* Clarendon Press, 1961.

[2] C.T.H. Baker, L. Fox, D.F. Mayers, and K. Wright. Numerical solution of Fredholm integral equations of first kind. *Computer Journal*, 7:141–147, 1964.

[3] R.J.S. Brown, G.C. Borgia, P. Fantazzini, and E. Mesini. Problems in identifying multimodal distributions of relaxation times for NMR in porous media. *Magnetic Resonance Imaging*, 9:687–693, 1991.

[4] J.P. Butler, J.A. Reeds, and S.V. Dawson. Estimating solutions of first kind integral equations with non-negative constraints and optimal smoothing. *S.I.A.M. Journal on Numerical Analysis*, 18:381–397, 1981.

[5] D.V. Ellis. *Well Logging for Earth Scientists.* Elsevier Scientific Publishing Company, 1987.

[6] T.C. Farrar and E.D. Becker. *Pulse and Fourier Transform NMR.* Academic Press, 1971.

[7] R. Freedman. A signal processing algorithm for the pulsed nuclear magnetism t ol. Technical report, Schlumberger Houston Product Center, June 1992.

[8] D.P. Gallegos and D.M. Smith. A NMR technique for the analysis of pore structure: Determination of continuous pore size distributions. *Journal of Colloid and Interface Science*, 122:143–153, 1988.

[9] A.A. Giordano and F.M. Hsu. *Least Square Estimation with Applications to Digital Signal Processing.* John Wiley & Sons, 1985.

[10] S.H. Gould. *Variational Methods for Eigenvalue Problems, Mathematical Expositions No. 10.* University of Toronto Press, 1957.

[11] C.W. Groetsch. *The theory of Tikhonov regularization for Fredholm equations of the first kind. - (Research notes in mathematics; 105).* Pitman Advanced Publishing Program, 1984.

[12] R.L. Kleinberg, A. Sezginer, D.D. Griffin, and M. Fukuhara. Novel NMR apparatus for investigating an external sample. *Journal of Magnetic Resonance*, 97:466–485, 1992.

[13] L.L. Latour, R.L. Kleinberg, and A. Sezginer. Nuclear magnetic resonance properties of rocks at elevated temperatures. *Journal of Colloid and Interface Science*, 150(2):535–548, 1992.

[14] G.F. Miller. *Numerical Solution of Integral Equations*, chapter 13. Clarendon Press, 1974.

[15] K. Overloop and L. Van Gerven. NMR relaxation in adsorbed water. *Journal of Magnetic Resonance*, 100:303–315, 1992.

[16] B.L. Phillips. A technique for the numerical solution of certain integral equations of the first kind. *Journal Association for Computing Machinery*, 9:84–97, 1962.

[17] A. Sezginer. An algorithm to process downhole pulsed-NMR measurements. Technical Report EMG–002–92–35, Schlumberger-Doll Research, June 1992.

[18] G. Strang. *Linear Algebra and its Applications.* Academic Press, 1976.

[19] A.N. Tikhonov. Regularization of incorrectly posed problems. *Soviet Mathematics Doklady*, 4:1624–1627, 1963.

[20] A.N. Tikhonov. Solution of incorrectly formulated problems and the regularization method. *Soviet Mathematics*, 4:1035–1038, 1967.

[21] A.N. Tikhonov and V.Y. Arsenin. *Solutions of Ill-posed Problems.* John Wiley & Sons, Inc., 1977.

[22] H.L. Van Trees. *Detection, Estimation, and Modulation Theory, Part I.* John Wiley & Sons, Inc., 1968.

[23] S. Twomey. On the numerical solution of fredholm integral equations of the first kind by the inversion of the linear system produced by quadrature. *Journal Association for Computing Machinery*, 10, 1963.

[24] S. Twomey. *Introduction to the Mathematics of Inversion in Remote Sensing and Indirect Measurements.* Elsevier Scientific Publishing Company, 1977.